

Spatiotemporally resolved imaging of streamer discharges in air generated in a wire-cylinder reactor with (sub)nanosecond voltage pulses

This content has been downloaded from IOPscience. Please scroll down to see the full text.

2017 Plasma Sources Sci. Technol. 26 075009

(<http://iopscience.iop.org/0963-0252/26/7/075009>)

View [the table of contents for this issue](#), or go to the [journal homepage](#) for more

Download details:

IP Address: 131.155.2.68

This content was downloaded on 04/07/2017 at 16:34

Please note that [terms and conditions apply](#).

Spatiotemporally resolved imaging of streamer discharges in air generated in a wire-cylinder reactor with (sub)nanosecond voltage pulses

T Huiskamp, W Sengers, F J C M Beckers, S Nijdam, U Ebert,
E J M van Hesch and A J M Pemen

Department of Electrical Engineering, Electrical Energy Systems group, Eindhoven University of Technology, PO Box 513, 5600 MB Eindhoven, The Netherlands

E-mail: t.huiskamp@tue.nl

Received 25 January 2017, revised 12 May 2017

Accepted for publication 30 May 2017

Published 4 July 2017



Abstract

We use (sub)nanosecond high-voltage pulses to generate streamers in atmospheric-pressure air in a wire-cylinder reactor. We study the effect of reactor length, pulse duration, pulse amplitude, pulse polarity, and pulse rise time on the streamer development, specifically on the streamer distribution in the reactor to relate it to plasma-processing results. We use ICCD imaging with a fully automated setup that can image the streamers in the entire corona-plasma reactor. From the images, we calculate streamer lengths and velocities. We also develop a circuit simulation model of the reactor to support the analysis of the streamer development. The results show how the propagation of the high-voltage pulse through the reactor determines the streamer development. As the pulse travels through the reactor, it generates streamers and attenuates and disperses. At the end of the reactor, it reflects and adds to itself. The local voltage on the wire together with the voltage rise time determine the streamer velocities, and the pulse duration the consequent maximal streamer length.

Keywords: streamer discharges, pulsed corona plasma, ICCD imaging, nanosecond pulsed power

1. Introduction

Pulsed power technology is often used to generate gas discharges, such as a pulsed corona discharge, which can be used for efficient air purification applications [1]. This discharge comprises multiple parallel filaments, called streamers. Streamers typically have a velocity in the range of 10^5 – 10^7 m s⁻¹ and a diameter of several hundred micrometres to several millimetres [2–12]. By using pulsed high voltage to generate the streamer discharge, the bulk gas remains cold and therefore such a discharge is often referred to as ‘non-thermal plasma’. Besides the pulsed streamer discharge, other types of non-thermal plasmas include (RF) dielectric barrier discharges (DBD), plasma jets and gliding arc discharges [1]. Due to the high energetic electrons that are generated in non-

thermal plasmas, they are efficient in producing highly reactive radical species [1, 13], which makes them ideal for applications such as pollution control and material surface engineering [13, 14]. In our research, we mainly consider non-thermal plasma for air-purification applications [15].

Previous research shows that non-thermal plasmas generated by very short (nanosecond) high-voltage pulses are very efficient for a variety of air-purification applications [16–23]. Overall, researchers have noted that the pulse duration of the applied high-voltage pulse has a significant influence on the radical yield; shorter pulses result in higher yields [16–18, 22]. To study and understand this phenomenon, we have developed a flexible nanosecond pulse source that produces (sub)nanosecond pulses [24–27]. The output pulses from this nanosecond pulse source have an adjustable

amplitude of up to 50 kV (positive and negative), an adjustable pulse duration of 0.5–10 ns and a rise time of less than 200 ps.

In this paper we investigate the development of streamers in a wire-cylinder reactor (plasma reactor) as a function of time and position in the reactor. These streamers will be generated by applying the high-voltage pulses from our nanosecond pulse source to the wire electrode. When our (sub)nanosecond pulses are used, components like the plasma reactor behave like transmission lines, where transmission times and reflections become important. Therefore, the development of the streamers will be dictated by the pulse propagation (and dissipation) and reflections in the reactor. Consequently, the streamer development changes on very short time scales and will depend on the position in the reactor.

The main motivation to study the development of streamers in our corona-plasma reactor is that we have to visualise the streamer discharge to understand and explain the plasma-processing measurements that are performed in the plasma reactor (the topic of [15], ch 8). Specifically, we are interested in the distribution of the streamers in the reactor, because the high-energy electrons and therefore the radicals needed for air-purification processes are generated in the streamer head and the path of the streamer [28–34]. Therefore, the distribution of the streamers in the reactor directly influences the chemical activity in the reactor. However, when the streamers cross the gap between the electrodes, secondary streamers can form [5, 6, 30, 35]. The electrons in the secondary streamers are less energetic—typically only 1–2 eV as compared to 5–10 eV for primary streamers—and consequently the radical generation in these streamers is different than in primary streamers [5, 6]. For example, some studies show that the energy yield of oxygen radicals is highest in the primary streamer phase [16, 29], whereas others claim a higher oxygen-radical energy yield in the secondary streamer phase [36, 37]. Therefore, to investigate this further, we want to optimise the streamer distribution such that the streamers should be as long as possible (and therefore occupy the most space in the reactor) without generating secondary streamers.

1.1. Streamer development

1.1.1. Streamer propagation velocity. There are many studies on streamer development under pulsed voltage conditions [2–12, 22, 38–48]. For instance, several researchers have reported on streamer propagation velocities for a range of voltages and rise times. This streamer propagation velocity is an important parameter for the streamer discharge in our coaxial reactor because it determines how far a streamer can propagate and therefore influences the distribution of the streamers in the plasma reactor. It is generally found and understood that a higher applied electric field increases the streamer propagation velocity and that the velocities are in the range of 10^5 – 10^7 m s⁻¹ [2–6, 9, 11, 12, 47]. Furthermore, various experiments show that negative streamers generally have a lower propagation velocity than positive streamers

[6, 10, 12, 40, 45, 47, 48], which is surprising because negative streamers propagate through electron drift and positive streamers propagate against the electron drift through photoionisation (and to a lesser extent background ionisation) [9, 38, 49]. Therefore, for identical field enhancement at the streamer head, and a similar electron distribution, a negative streamer is expected to propagate faster [50]. Luque *et al* showed that negative streamers indeed travel faster initially, but that due to broadening of the streamer head, the field enhancement at the streamer head decreases, which decreases its velocity [46]. At the same time, the positive streamer head remains smaller during propagation and therefore the field enhancement remains higher, leading to a faster velocity of the positive streamer.

Besides the applied voltage amplitude, the rise rate of the applied voltage also influences the streamer propagation velocity. Most studies found that the velocity increases when the rise rate increases [6, 41, 42, 45, 48, 51]. This effect was explained by the fact that streamers initiate while the high-voltage pulse still rises and therefore initiate at a lower voltage when the rise rate is low.

1.1.2. Electrode geometry. The electrode geometries of the experimental setups in which researchers have studied streamer development vary. The majority have used point-plate geometries which are very useful for fundamental streamer research because of optical accessibility and reproducibility [3–5, 8–10, 22, 38–40, 43, 44, 47]. Some used wire-plate geometries [6, 7] and only a few have looked at coaxial geometries [2, 11, 12, 52]. The coaxial geometries are of interest because it is the electrode configuration that we use and that is employed by us and many others for air-purification research (e.g. [1, 53–59]). Unfortunately, most observations of the streamers in a coaxial geometry have only been done at one position in the plasma reactor and the effects of pulse propagation in the reactor have not been considered so far.

A study that includes the effects of pulse propagation on streamer development over a longer length of transmission line is the study by Pokryvailo *et al*, who used a 6 m long two-wire transmission line and generated a corona plasma with a 5 ns 100 kV pulse [60]. They found that the discharge light intensity decayed along the line and that this effect was more or less independent on the applied voltage. However, no information was given on any discharge parameters.

Another study that considers the propagation of a high-voltage pulse when a discharge is generated was performed by Van Heesch *et al* [61]. They used a coaxial reactor for pulsed corona experiments and monitored the pulse with electrical measurements (no imaging measurements) for a pulse with a 5 ns rise time and found that the pulse attenuated severely over 4 m due to the corona discharge.

Finally, Beckers investigated the energy dissipation in a 4.5 m corona reactor and found that in the end of the reactor, more energy was dissipated than in the beginning and middle of the reactor [62]. This is an indication that the streamer

discharge varies along the reactor, which is due to the effects of pulse propagation through the reactor.

In this paper, we will also study the effect of the pulse propagation through a transmission-line system with very short pulses, but we will show streamer parameters such as the streamer distance travelled and the streamer velocity as a function of time and position in the coaxial reactor. In this way we get an insightful view on nanosecond transient plasma generation in a coaxial corona-plasma reactor.

1.2. Paper organisation

After this introduction, section 2 presents the experimental setup we used in this paper, followed by section 3 in which we show a SPICE (Simulation Program with Integrated Circuit Emphasis) model of the corona-plasma reactor to model the voltage waveforms in the reactor as a function of time and position in the reactor. Sections 4 and 5 are the first two results sections in which we show results of ICCD-imaging experiments for different pulse-source parameters in a 2 m reactor and a 1 m reactor respectively. Subsequently, section 6 shows results of similar experiments, but then with the rise time of the applied pulses as the main variable. Finally, section 7 presents the conclusions.

2. Experimental setup and procedure

The streamer development in our corona-plasma reactor is driven by the propagation of the very short pulses through the reactor. Therefore, we need to be able to visualise the streamers both as a function of time as well as a function of position in the reactor. We use ICCD photography to capture individual images (of streamers generated with individual pulses) and later join them together to generate an overview of the entire reactor. This results in a significant amount of experiments and data, which is why the experiments are automated. With the images we study the streamer development as a function of the pulse duration, pulse voltage, pulse polarity and pulse rise time.

The experimental setup we used for the experiments in this paper was the subject of previous papers [26, 63] and will be shortly summarised here.

2.1. Nanosecond pulse source and sensors

We recently developed the nanosecond pulse source we used for the experiments in this paper at Eindhoven University of Technology. It is a single line pulse source, consisting of a pulse forming line that is charged by a microsecond pulse charger and is subsequently discharged by an oil spark gap. The generated pulse travels over a transmission line (a SA24272 coaxial cable) to the load, the corona reactor, where it produces a sufficiently high electric field to generate a streamer discharge. The coaxial cable adds a delay to the high-voltage pulses and is required to synchronise the ICCD camera with the generated high-voltage pulses. The full design of this system is described in [24–27] and is

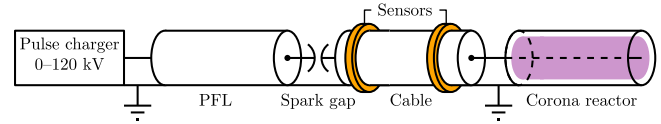


Figure 1. Schematic of the single line pulse source. The pulse charger charges the pulse forming line (PFL) which is then discharged by the spark gap into a matched cable. When the voltage pulse reaches the corona reactor it generates a streamer discharge. B-dot and D-dot sensors are integrated on the cable to measure voltage and current waveforms Reprinted with permission from [63]. Copyright (2016), AIP Publishing LLC.

schematically presented in figure 1. The output pulses from the nanosecond pulse source ($50\ \Omega$ output impedance) have an adjustable amplitude of 3–50 kV (positive and negative), an adjustable pulse duration of 0.5–10 ns and a rise time of less than 200 ps. Figure 2 shows some example waveforms.

The pulse generation process is controlled by the microsecond pulse charger and its power supply, which is in turn controlled by software on a computer. This allows for full automation of the nanosecond pulse source once the required spark-gap distance and PFL length are set by hand.

On the SA24272 coaxial cable that connects the plasma reactor to the pulse source, we mounted B-dot and D-dot sensors to measure the current and voltage of the high-voltage pulses respectively [64]. Four sensors are mounted on the side of the plasma reactor (D_3 , D_4 , B_3 and B_4) and two on the pulse source side (D_5 and B_5). For example, the waveforms of figure 2 were measured with sensor D_5 .

2.2. Plasma reactor and imaging system

The plasma reactor is connected to the end of the SA24272 coaxial cable. This connection is made with a cable coupler, that was designed to be impedance matched to the coaxial cable and was introduced in [65].

Normally, we use a coaxial plasma reactor for our plasma processing experiments. However, for our imaging experiments we require good optical access to the entire streamer discharge. Therefore, we use a plasma reactor that has a window along its entire length, but is in every other way similar to the coaxial reactor. Figure 3 shows this reactor. It is 1 m long and two of these reactors can be connected in series to create a 2 m long reactor. The reactor has a gas-tight polycarbonate (PC) window to allow imaging of the streamers. The U-shaped reactor can be connected to the cable coupler on the SA24272 cable in the same way as our normal coaxial reactor.

We used a 4 Picos-DIG ICCD camera from Stanford Computer Optics to image the discharge. It has a minimum exposure time of 200 ps and its CCD has a resolution of 780×580 pixels. We attached a Sigma 70–300 F4–5.6 DG MACRO lens to the camera and enclosed it in a shielded cabinet. The spatial resolution of the camera is 0.1 mm per pixel and the depth of field of the images is around 10 mm. The camera is triggered by the D-dot sensor on the side of the nanosecond pulse source. This results in a trigger jitter of less than 100 ps.

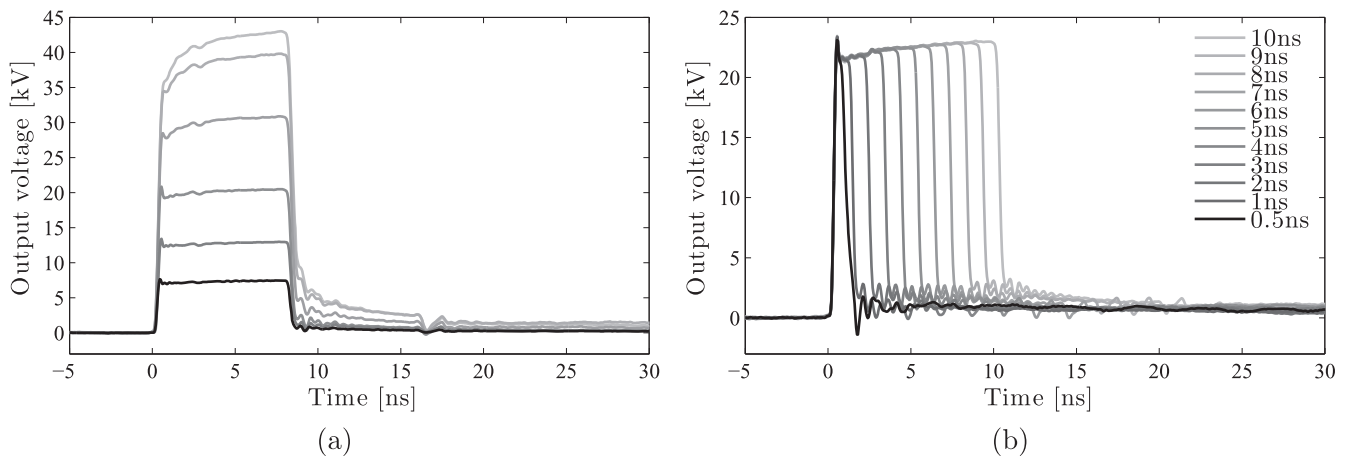


Figure 2. Example waveforms of the nanosecond pulse source. (a) A 8 ns pulse with different amplitudes. (b) A 22 kV pulse with different pulse durations.

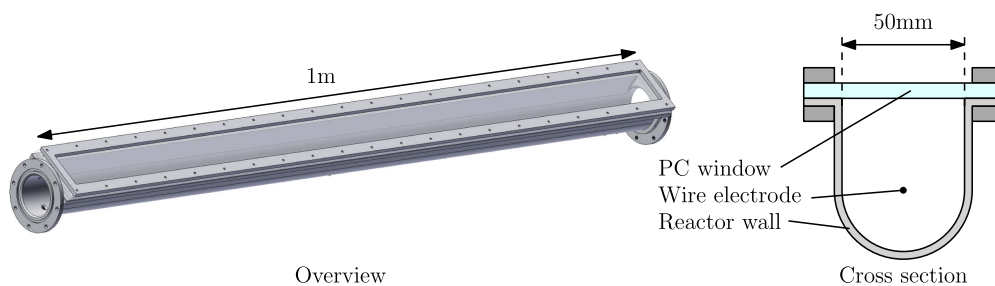


Figure 3. An overview drawing of the 1 m corona-plasma reactor with a polycarbonate window (left) and a cross section of this reactor (right). The reactor has a U-shaped cross section that allows the ICCD camera to image the inside of the reactor. Two of these 1 m reactors can be connected in series to obtain a 2 m long reactor. Reprinted with permission from [63]. Copyright (2016), AIP Publishing LLC.

The camera is mounted on rails in a large aluminium frame. The U-shaped reactor hangs from the top of the frame in line with the rails over which the camera moves. It is positioned in such a way that the camera can look into the reactor via a mirror and image a part of it.

The computer that controls the pulse generation of the pulse source also controls a stepper motor that moves the cabinet with the camera over the rails. In this way, the computer controls the camera position. The camera moves over the rails in what we define as the x direction (where $x = 0$ is the end of the reactor furthest away from the pulse source side). The control sequence is now as follows: the computer sends the camera to the first x -position and generates 20 pulses (for averaging purposes¹), while for each pulse the camera takes an image at user specified settings. Then the shutter delay of the camera is increased and again 20 images are taken. This repeats until all shutter delays are done. Then the camera is moved to the next x -position (38 positions in total for a 2 m reactor). In this way, the entire reactor is imaged in small steps in position and in time. After this procedure, two different steps are applied. In the first step, streamer parameters are calculated for each individual image (see next section). For the second step the images are

¹ This averaging is required because the amplitude of the output voltage of the nanosecond pulse source is not exactly the same for each pulse. This standard deviation on the amplitude (around 10% of the average amplitude) is caused by the oil spark gap in the pulse source (see [24]).

averaged and joined together to produce images of the entire reactor for different instances in time.

2.3. Data processing

Besides joining the data to form images of the entire reactor, the most important processing that is undertaken on the images is the determination of the streamer lengths (the distance from the HV-wire to the tip of the streamer head) with a script. It loads each image (figure 4(a)) and generates a filtered streamer profile from each image (figure 5). Since our geometry is 3D, streamers will not only propagate in the plane of focus, but also in other directions. Therefore, the script determines the streamer length as the longest peak in the filtered streamer profile, because this will be the streamer that propagates in the plane of focus. The streamer length data that is presented in this paper always uses the average of the maximum streamer lengths determined for all 20 images at each position (and for each shutter delay). The full details of this method are described in [63].

2.4. Rise-time variation

One of the parameters of the high-voltage pulses we vary is the rise time. This is implemented by introducing a capacitor in parallel with the reactor. This capacitor is mounted at the beginning of the reactor to change the pulse that propagates into the reactor. The capacitor comprises in-series-connected

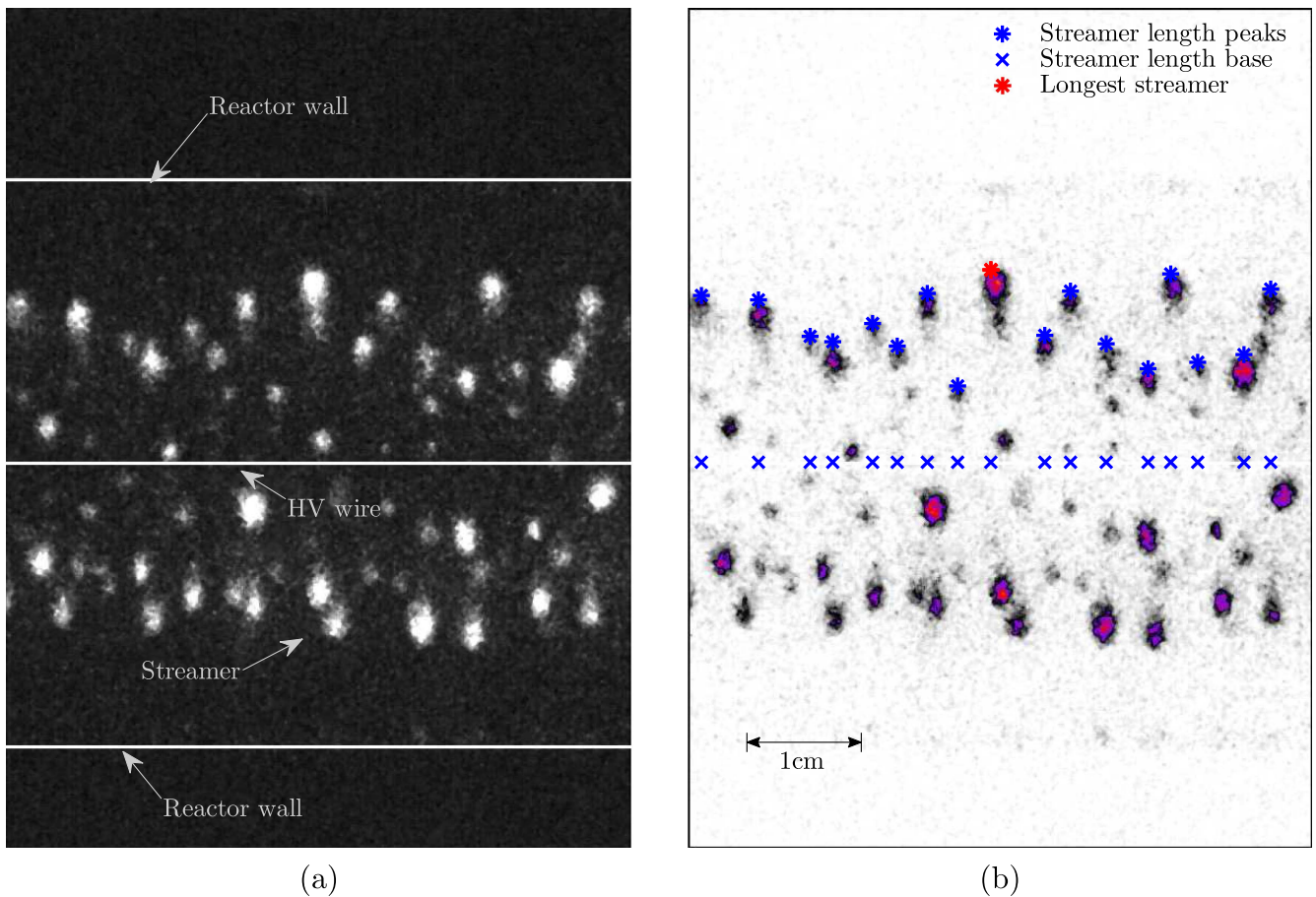


Figure 4. An example of how the raw images are processed. The raw image in (a) is taken near the end of the reactor for a 9 ns pulse, a camera delay of 9 ns and a voltage of 36 kV. In (a) the software added lines for the reactor wall and the high-voltage wire. The bright dots are the heads of the streamers. (b) The automated script detects the position of the streamers from a filtered streamer profile (see figure 5). This streamer profile is generated from the image by applying a brightness-threshold. We applied a colour map to the raw image for clarity.

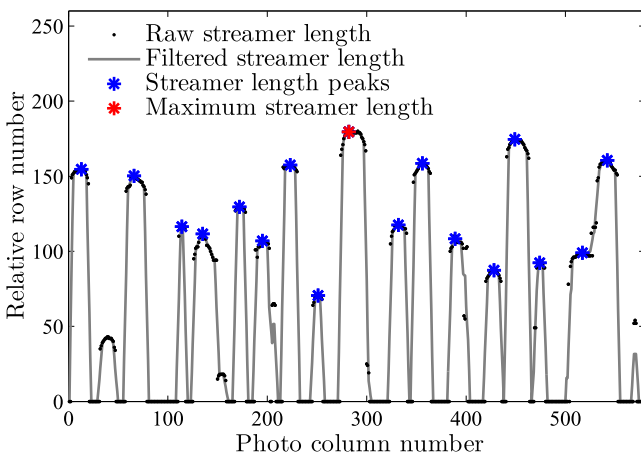


Figure 5. The streamer lengths are calculated from the filtered profile as the local maxima.

100 pF 10 kV capacitors. In the experiments of this paper we use three configurations: no capacitors, a string of three capacitors in series resulting in a total capacitance of 33 pF and two parallel strings of three capacitors in series resulting in a total capacitance of 67 pF. More details on can be found in [15, section 6.2.5].

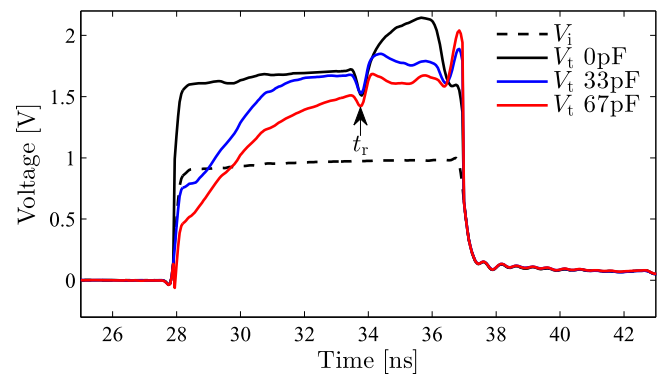


Figure 6. The rise-time variation of the 9 ns pulse (transmitted waveforms (normalised to the amplitude of the input pulse) in the reactor calculated from measurements). By adding capacitors in the corona-plasma reactor we can achieve a rise-time of 0.4 ns (no capacitor), 2.9 ns (33 pF) and 5.6 ns (67 pF). The waveforms after time t_r should be ignored because the calculated waveforms are no longer the real transmitted waveforms.

It is not possible to measure the waveforms in the real reactor directly, but the applied reactor waveform can be found indirectly from the incident and reflected pulse, as we described in [65]. Waveform V_i is the transmitted waveform (the waveform applied inside the reactor) that can be calculated

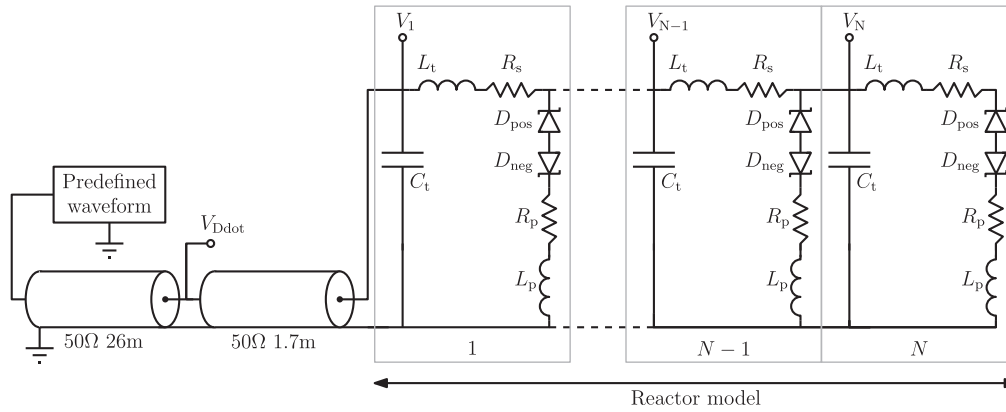


Figure 7. The SPICE model of the corona-plasma reactor. It consists of N sections of distributed transmission lines with a dissipative branch in addition to the standard transmission-line components. The dissipative branch models the dissipation by the streamers and consists of a resistor switched by Zener diodes. Two ideal transmission lines (left side) model the SA24272 cable that connects the pulse source to the reactor. The pulse source is modelled with a pre-defined waveform.

from the incident waveform and the reflected waveform. If we apply this method to measurements on the reactor with the capacitors we find the waveforms of figure 6. The waveforms after time t_r are not purely the applied waveforms anymore, because at this time the transmitted pulse has travelled up and down the reactor and adds to itself. However, if we consider the waveforms up to t_r we find (10%–90%) rise times of 0.4 ns (no capacitor), 2.9 ns (33 pF) and 5.6 ns (67 pF).

3. Reactor SPICE model

We developed a SPICE model in LTspice [66] of the reactor to better understand the development of the streamers in the corona-plasma reactor. The model we developed is a simple transmission line model with dissipative components to approximate the dissipation by the streamers. Therefore, this model is not meant as an exhaustive discharge model, but rather as a simple electrical equivalent model of the reactor and the streamers. It will allow us to derive an approximation of the voltage waveforms inside the reactor to understand what transmission-line effects will be relevant for the streamer development. For a more complete model, methods such as used in e.g. [67] or [68] could be implemented.

3.1. SPICE model

The SPICE model of the coaxial (wire-cylinder) corona-plasma reactor is shown in figure 7. It consists of N identical sections with lumped elements that make up the transmission line elements of the reactor. Each section contains a distributed capacitance C_t and a distributed inductance L_t . The distributed capacitance is calculated with

$$C_t = \frac{2\pi\epsilon_0 l_r}{N \ln \frac{d_o}{d_i}}, \quad (1)$$

where l_r is the length of the reactor, d_o and d_i are the outer and inner conductor diameters of the reactor respectively and N is the number of sections in the model. Similarly we can define

the distributed inductance as

$$L_t = \frac{\mu_0 l_r}{2\pi N} \ln \frac{d_o}{d_i}. \quad (2)$$

The distributed resistance of the wire in the reactor is represented by R_s in the SPICE model. It is calculated as the resistance of the outer shell of the wire that is bounded by the skin depth δ and is calculated with

$$R_s = \frac{l_r}{\sigma_{ss} [d_i^2 - (d_i - \delta)^2] \pi N}, \quad (3)$$

where σ_{ss} is the conductivity of the stainless-steel wire and δ is calculated as

$$\delta = \sqrt{\frac{1}{\pi f \mu_0 \sigma_{ss}}}, \quad (4)$$

where f is the frequency at which the skin depth is considered.

The distributed components C_t , L_t and R_s are the classical parameters of a transmission line (with losses in the dielectric neglected) [69].

We added a resistive load R_p to model the dissipation of the streamers in the reactor. We can verify the validity of the use of a resistor as a simple model for a streamer discharge by looking at the results of figure 7 in [65], which shows that the dissipated plasma energy increases with the square of the applied voltage. This is similar to the energy dissipation of a resistor.

In the real reactor, the discharge initiates only after a certain voltage threshold has been crossed: the inception voltage [70]. We model this behaviour with a Zener diode (just as was done in, e.g. [67, 71]), because a Zener diode starts conducting above a certain voltage V_{br} . When the Zener diode is conducting, a current will flow through the resistive load R_p , which results in energy dissipation in this resistor (and the Zener diode). Therefore, the combination of the Zener diode in series with a resistor models the streamers: above an inception voltage the streamers will dissipate energy proportional to the square of the voltage. Furthermore, we used two Zener diodes in each branch to differentiate between the positive and negative inception voltage of the streamers.

Table 1. SPICE model parameters for a 1 m reactor.

Parameter	Value	Parameter	Value
N	128	L_p	1.5 nH
l_r	1 m	R_s	0.1 Ω
d_o	50 mm	R_p	22.5 k Ω
d_i	0.5 mm	$V_{br,pos}$	4 kV
C_t	93.8 fF	$V_{br,neg}$	6 kV
L_t	7.2 nH		

The last component in the SPICE model of the reactor is the inductor L_p in series with R_p . We placed this inductor in series with R_p because in the real discharge, a streamer needs time to develop. The longer a high-voltage pulse is applied, the further the streamer propagates and the more energy is dissipated. Inductor L_p ensures that more energy can be dissipated in R_p when a longer pulse is applied, because the rate with which the current through the resistor can increase is now determined by the inductor.

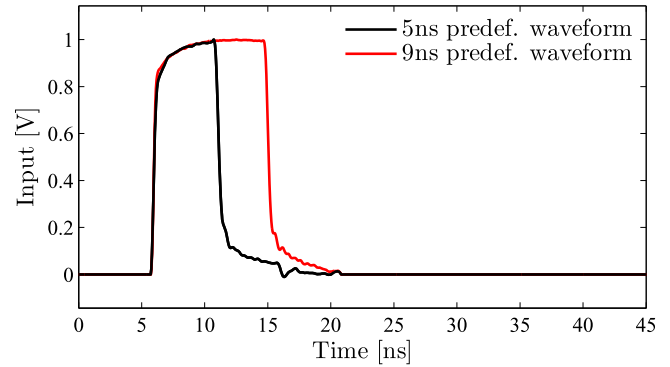
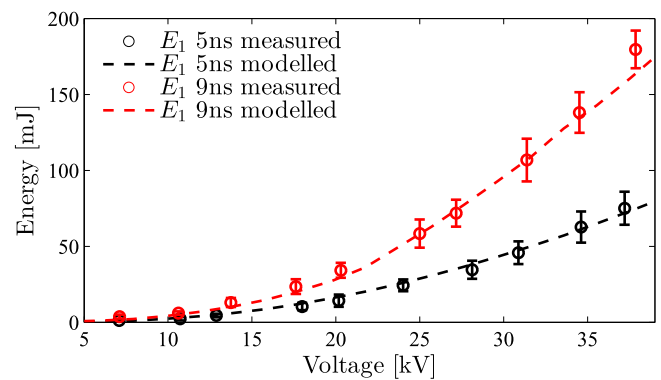
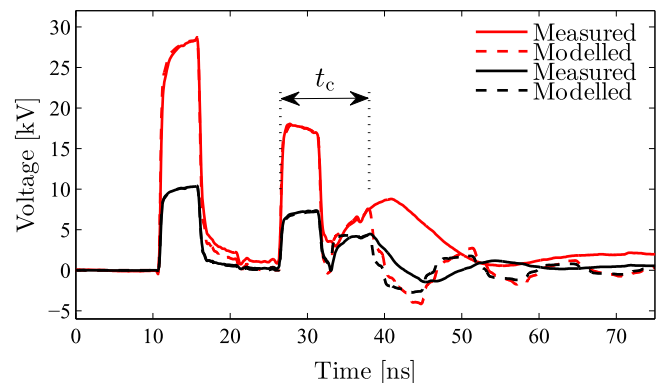
Table 1 lists all the relevant parameters of the SPICE model for a 1 m reactor. We used a model with 128 sections. If we consider that the pulse travels with the speed of light through the reactor, then one section represents $1/128 \times 1/3 \times 10^8 = 26$ ps of pulse propagation, which is around one order of magnitude shorter than the rise time of the pulses. Therefore, using $N = 128$ is allowed.

The physical parameters of the reactor (l_r , d_i and d_o) give the transmission-line parameters C_t and L_t . With a frequency of around 100 MHz (the main average frequency component of the 5–9 ns pulses) we then find a value of around 0.1 Ω for R_s . Subsequently, we varied values for L_p , R_p and the breakdown voltages of the Zener diodes ($V_{br,pos}$ for D_{pos} and $V_{br,neg}$ for D_{neg}) to fit the experimentally measured energy dissipation by the discharge.

The total SPICE model of figure 7 consists of the 1 m reactor model and two transmission lines that represent the SA24272 cable. These transmission lines are ideal and have the same time delay as the real cables. In the real setup we measure the voltages and currents in the system with D-dot and B-dot sensors [64] mounted on the coaxial cable at 1.7 m from the reactor. We simulate this by measuring the voltage V_{Ddot} in the simulation at the interface of the two 50 Ω cables (see figure 7). Additionally, we measure the current at the same point to calculate the energy that is dissipated in the simulation. The two transmission lines are excited with a predefined waveform. This waveform is the actual pulse that was measured in experiments with D-dot sensors D_3 and D_4 in [65]. Figure 8 shows the predefined waveforms for a 5 and 9 ns pulse. To change the amplitude of the predefined waveform we scale the waveform.

3.2. Results

Figures 9 and 10 present comparisons between the experimental results and the modelled results. A very good agreement is found between the dissipated discharge energy for 5 and 9 ns pulses that we used in this example.


Figure 8. The predefined waveforms (normalised) that we used in the model of figure 7. These waveforms were taken from the experiments of [65].

Figure 9. A comparison between the modelled discharge energy dissipation (dotted lines) and the measured discharge energy dissipation (circles).

Figure 10. A comparison between the modelled waveforms and the experimental waveforms for a 5 ns pulse at two different output voltages.

Furthermore, figure 10 shows a measured and simulated voltage waveform measured with the sensors that are positioned on the cable 1.7 m from the corona-plasma reactor (in the real system, as well as in the simulation). Naturally, the incoming pulse (at $t = 10$ ns) is modelled faithfully, since the measured pulse is the input of the model. Then the pulse reflects on the cable-reactor interface and reappears at the sensors at $t \approx 25$ ns. The results show that the reflected pulse and therefore the impedance of the reactor is faithfully modelled (for at least the duration of the pulse). After the

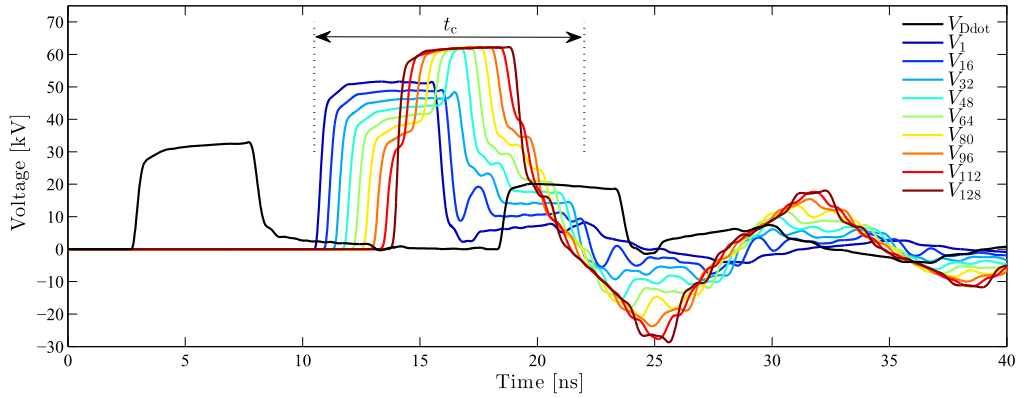


Figure 11. SPICE simulation results of the 1 m reactor. The waveforms are the voltages at various positions in the reactor (from V_1 at the pulse-source side of the reactor, to V_{128} at the end of the reactor). Noteworthy are the increased pulse amplitude due to mismatch when the incoming pulse (V_{Ddot}) enters the reactor and the voltage doubling at the end of the reactor.

reflected pulse, the model still shows good agreement for 6.5 ns longer. Consequently, the modelled and measured results show a good agreement for a total time of t_c (indicated in figure 10). After that time, the modelled results and the measured results start to deviate due to the complexity of the discharge behaviour and the modelling with a fixed value for R_p . Furthermore, the pulse has to propagate through the body of growing streamers, which also has significant effects on the pulse propagation and consequently changes the inductance of the system locally. After $t = 38$ ns the measured result shows a severely dispersed pulse, which is not correctly predicted by the SPICE model. The time window t_c is similar for the 9 ns pulses.

Figure 11 shows an example of the simulated voltage profiles in the reactor as a function of time and position. When the pulse enters the reactor it increases in voltage due to mismatch (V_1). It attenuates as it propagates through the reactor and finally reflects off the end of the reactor (V_{128}). Here it adds to the incoming pulse, causing a local doubling of the voltage. As the pulse propagates back towards the boundary of the transmission line and the reactor, it continues to add to the incoming wave until it reaches the boundary. In the real reactor, the pulse will already be very dispersed at this point and therefore these later stages of pulse reflections in the SPICE results will not be so significant.

We will use the voltage profiles of the SPICE simulations in the discussion of the results of this paper.

3.3. Rise-time variation

In the previous section we introduced a method of changing the rise time of the pulses that are applied to the corona-plasma reactor by adding capacitors in parallel to the reactor. Figure 12 shows the simulated transmitted waveforms when we add these capacitors to the SPICE model of our reactor. The results show that a successful change in the rise time can be realised.

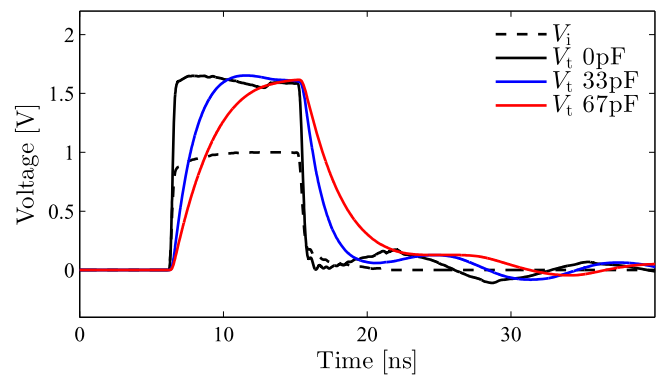


Figure 12. The simulated rise-time variation (normalised to the amplitude of the input pulse) of the 9 ns pulse obtained by adding capacitors in the corona-plasma reactor.

4. Results: pulse duration variation in a 2 m reactor

Here we present the results on the streamer development in a 2 m reactor with the pulse duration of the pulse source as the main parameter under investigation. For all experiments in this paper, we flushed the plasma reactor with synthetic air at atmospheric pressure at a flow rate of 5 L min^{-1} . Moreover, the repetition rate of the pulse source was 3 Hz.

We started with a 2 m reactor because a long reactor gives more insight in the development of the streamers with respect to the propagation of the pulse in the reactor. We used positive and negative pulses in the reactor with a pulse duration Δt of 1, 5 and 9 ns. The output voltage during each experiment (fixed polarity and Δt) was fixed and set with the spark-gap distance of the nanosecond pulse source. Between different experiments there are slight differences in this fixed output voltage because of slight differences in the spark-gap distance required for each experiment. The shutter delay t_d for the 2 m experiments was increased in steps of 2 ns and the exposure time t_e of the camera was 1 ns for the 1 and 9 ns experiments and 2 ns for the 5 ns experiments. The gain U_g of the camera was fixed at 980 V for all experiments in this section. Furthermore, the time line that we use for all the

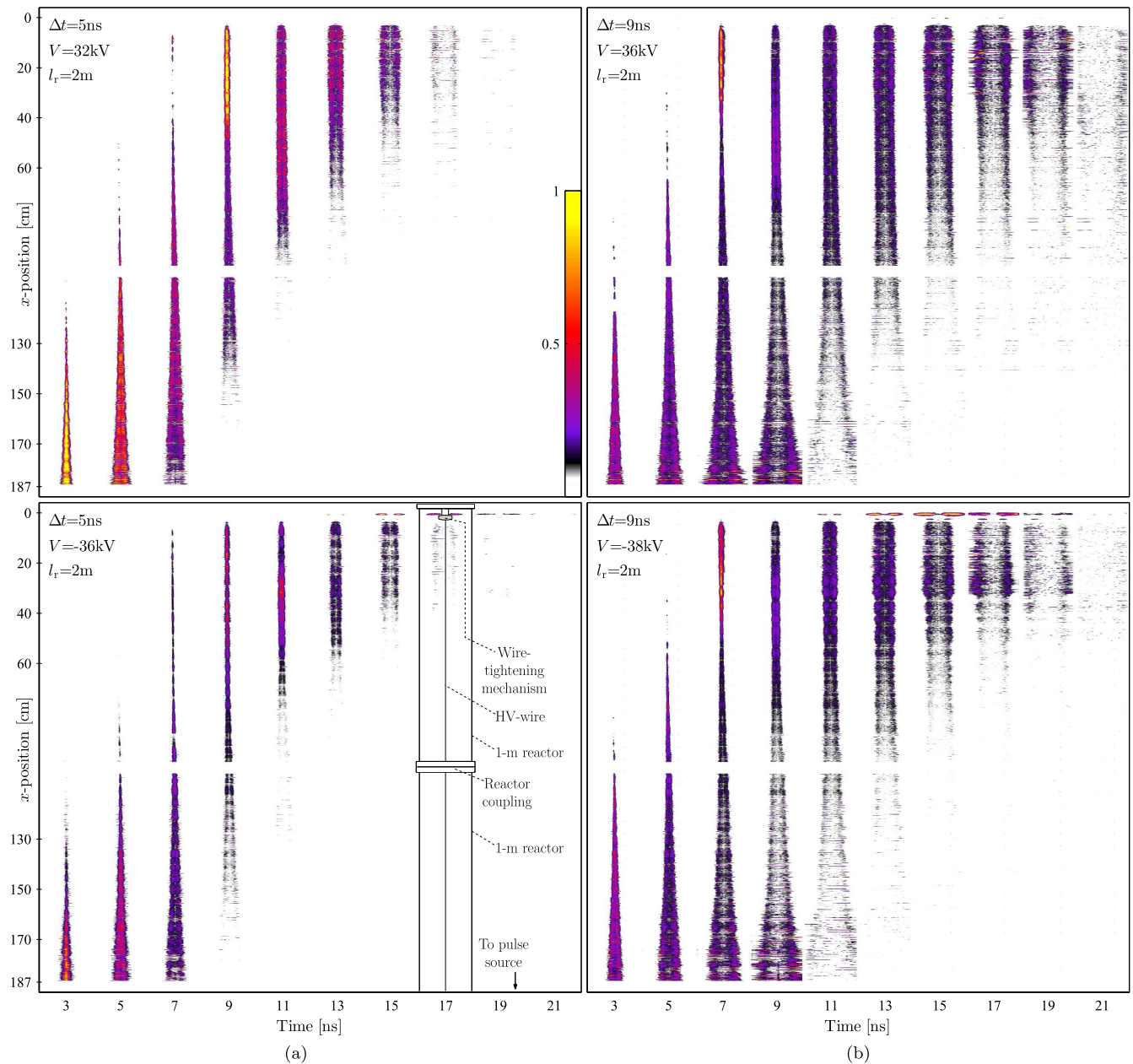


Figure 13. Streamer development in time for (a) a 5 ns positive (top) and negative (bottom) pulse and (b) a 9 ns positive (top) and negative (bottom) pulse in a 2 m reactor. The exposure time of the 5 ns images and 9 ns images is 2 ns and 1 ns respectively and each image is the average of 20 photos at each position. The colour map in (a) will be used in all the ICCD images of this paper.

images in this paper have $t = 0$ as the time at which we observe the first light in the reactor.

4.1. ICCD images

We present the results of each of the 5 and 9 ns experiments as a series of images, each representing a moment in time and showing the entire reactor (see section 2.2 for details). Figure 13 shows the end result. In all the images, the bottom is the beginning of the reactor (the side of the SA24272 cable) and the top is the end of the reactor. The correspondence of the images with the reactor geometry is indicated at $t = 15$ ns in the negative 5 ns results.

When we look at either the 5 ns or the 9 ns images we can compare the brightness for negative and positive pulses and see that the negative streamers are slightly less bright than the positive streamers, indicating a slightly lower field enhancement at the tip of the negative streamers. The second observation is that the propagation of the voltage pulse through the reactor determines the development of the streamers. As the pulse moves through the reactor, so does the initiation of the streamers. If we assume that the pulse propagates with the speed of light through the reactor, then upon entering the reactor (at $x = 200$ cm, not shown in the image) it takes around 6.7 ns for the front of the pulse to reach the end of the reactor. Here it reflects and it takes

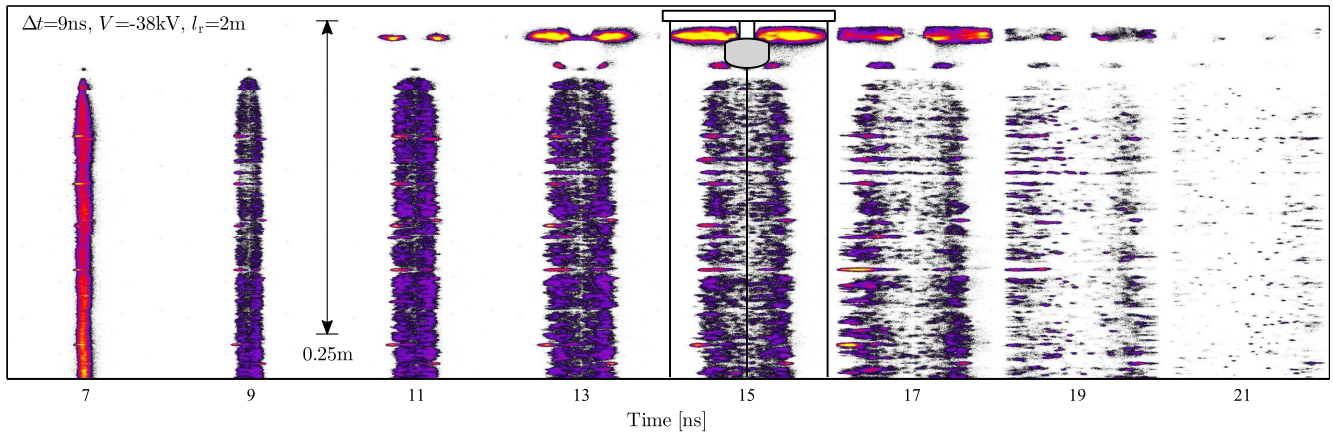


Figure 14. A close-up of the negative 9 ns discharges of figure 13. A bright discharge develops from the triple point caused by the metal-air-PVC interface of the wire-tightening mechanism behind the stainless-steel removable head. The image at $t = 15$ ns shows a sketch of this removable head and the reactor.

another 6.7 ns before the reflected front of the pulse reaches the beginning of the reactor again.

When we look at the bottom of each image (beginning of the reactor) it appears that after streamer initiation, the streamers propagate towards the wall of the reactor for a duration similar to the duration of the high-voltage pulse (Δt) before they extinguish. In other words: once the external electric field disappears, the streamers extinguish. At the end of the reactor (top of the image) the streamers propagate longer than just during the period of a pulse duration. This is caused by the reflection of the pulse at the end of the reactor and therefore, depending on the x -position, the external field is present for a longer time. In addition the total electric field is increased when the incoming pulse and the reflected pulse overlap. Both of these effects causes the increase in streamer length near the end of the reactor. We will look into this effect in more detail in the sections on the SPICE simulations and streamer length.

If we compare our results with the results of Pokryvailo *et al* [72], we note that the discharge-size decay that they observed for an increasing position along the wire is also present in our results. They attributed this decay to a decrease in the voltage amplitude along the wire, which is also the reason we observe the decay here. This decay in voltage along the transmission line when a discharge is present was also shown by Van Heesch *et al* [61]. In addition, our results also explain the findings of Beckers that the energy dissipation by the plasma is higher at the end of a corona plasma reactor [62].

4.1.1. Other observations. An interesting feature presents itself in figure 13 when we compare the results of the negative pulses with the results of the positive pulses: the bright discharge at the end of the reactor (top of the images). It is significantly present in the negative discharges. Figure 14 shows a closer look at the negative 9 ns results. This bright discharge is caused by the triple point formed by the wire-tightening mechanism of the reactor (shown at $t = 15$ ns). The body of this mechanism is made out of PVC (polyvinyl chloride) and has a stainless steel head that holds the HV wire of the reactor. At the back of the stainless-steel head, the metal meets the PVC and creates a triple point (metal—air—PVC)

and causes local electric field enhancement [73]. This triple point is where the thick streamers at the end of the reactor originate.

If we examine the images carefully (also the single images that are not shown here), we find no evidence of secondary streamers; all the streamers we observe appear to be primary streamers. Secondary streamers often appear as a glow on the wire electrode after the primary streamer crossed the gap [6, 22, 74].

Besides 5 and 9 ns experiments, we also performed experiments with a 1 ns pulse. However, these results mainly showed that a pulse duration of 1 ns hardly produces any discharge at all at the voltages we used. The voltage amplitude will have to be increased significantly (higher than 50 kV) before anything useful might be seen. Therefore, we leave the 1 ns experiments out of our study in this paper.

4.2. SPICE simulation

We used the SPICE model of the reactor of section 3 to simulate the voltage at each position in the reactor. We connected two of the reactor models in series to obtain a 2 m reactor model and adjusted the amplitude of the predefined waveform to the amplitude of the voltages that we used in the real experiments. We only model the positive results, because the SPICE model lacks the incorporation of the reactor-ended bright discharge at the end of the reactor. Figure 15 shows the results of the simulations and presents the voltage in the reactor at each position for different times.

The simulation results show that when the pulse enters the reactor it travels through the reactor and attenuates in time, until it reflects on the open end of the reactor, reverses direction and adds to the incoming pulse. Here we have to keep in mind that the simulation results only agree well up until around $t = 11.5$ ns as we saw in section 3.

4.3. Streamer length

One of the main motivations for the experiments of this paper is to study the effect of very short pulses on the distribution of

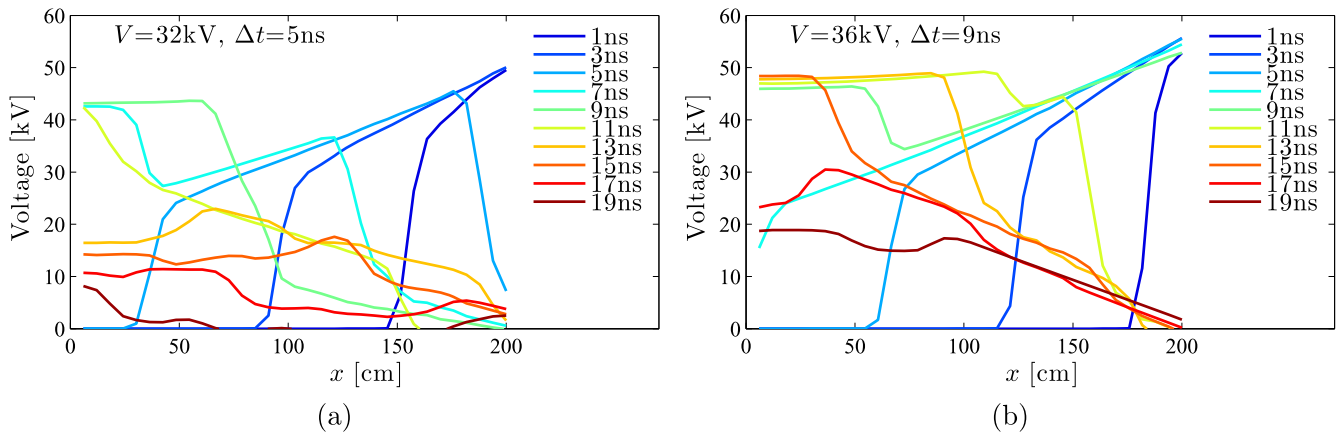


Figure 15. SPICE simulation results for (a) a 5 ns positive pulse and (b) a 9 ns positive pulse at the same applied pulse amplitude as in the 2 m reactor experiments. The figures show the voltage amplitude in the reactor at each position and as a function of time (presented similarly as the streamer lengths in figure 16).

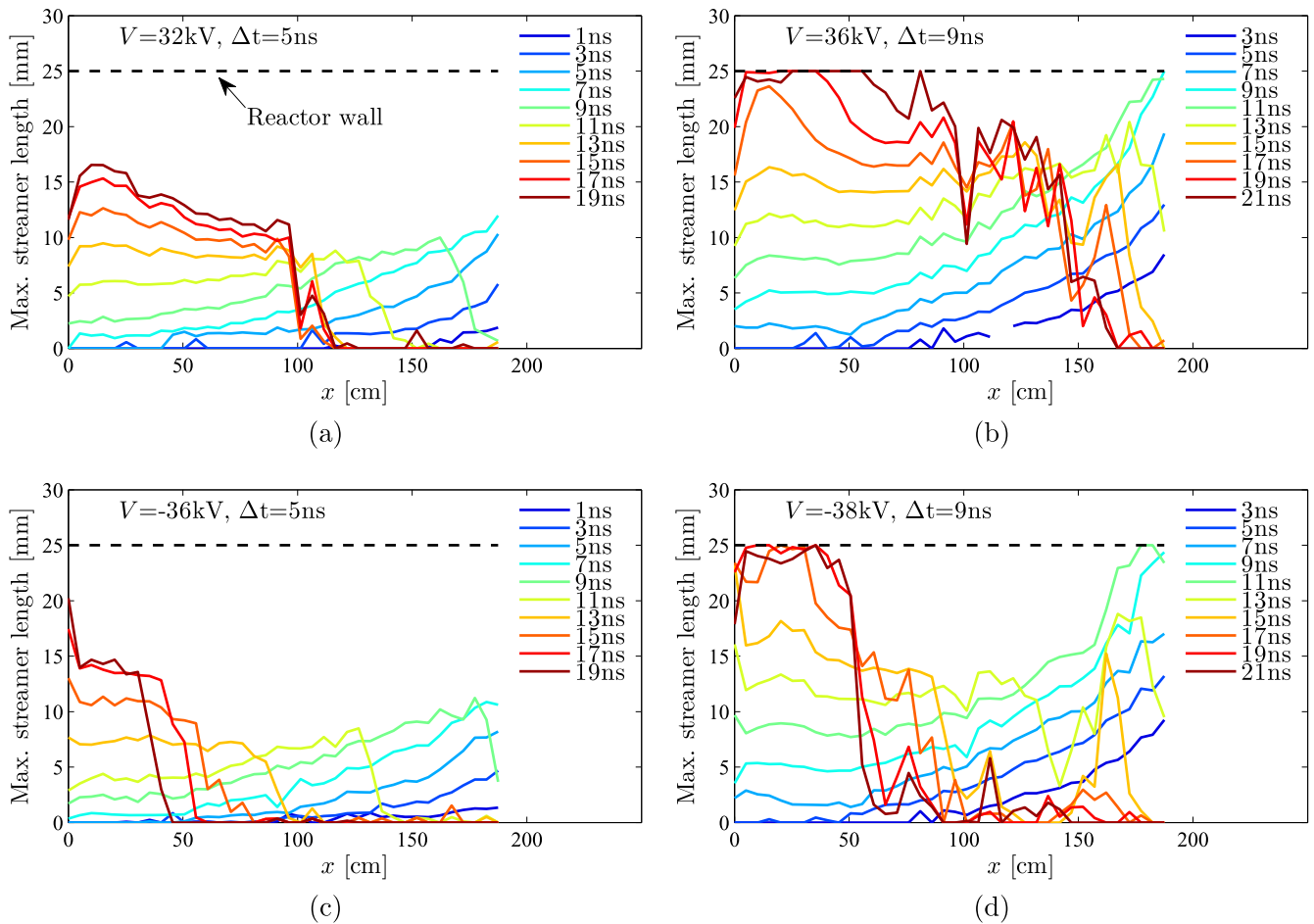


Figure 16. A quantitative representation of the maximum streamer lengths (averaged over the results from 20 photos at each position and each time) calculated from the results of figure 13 for (a) the positive 5 ns experiments, (b) the positive 9 ns results, (c) the negative 5 ns results and (d) the negative 9 ns results. The left side of each figure corresponds to the end of the reactor.

the streamers in the reactor. From the results so far we could see that this streamer distribution is not homogeneous at all times and at all positions in the reactor. To get a more quantitative evaluation of this distribution we look at the streamer length as a function of x -position and time, which is automatically calculated by the software. Figure 16 shows the

streamer lengths for the 5 and 9 ns experiments in the 2 m reactor.

If we first look at just figure 16(a), we see that the streamer length at each x -position becomes on average about 10–15 mm, but that this length is reached at very different times of the discharge. At the beginning of the reactor (high x -position) the

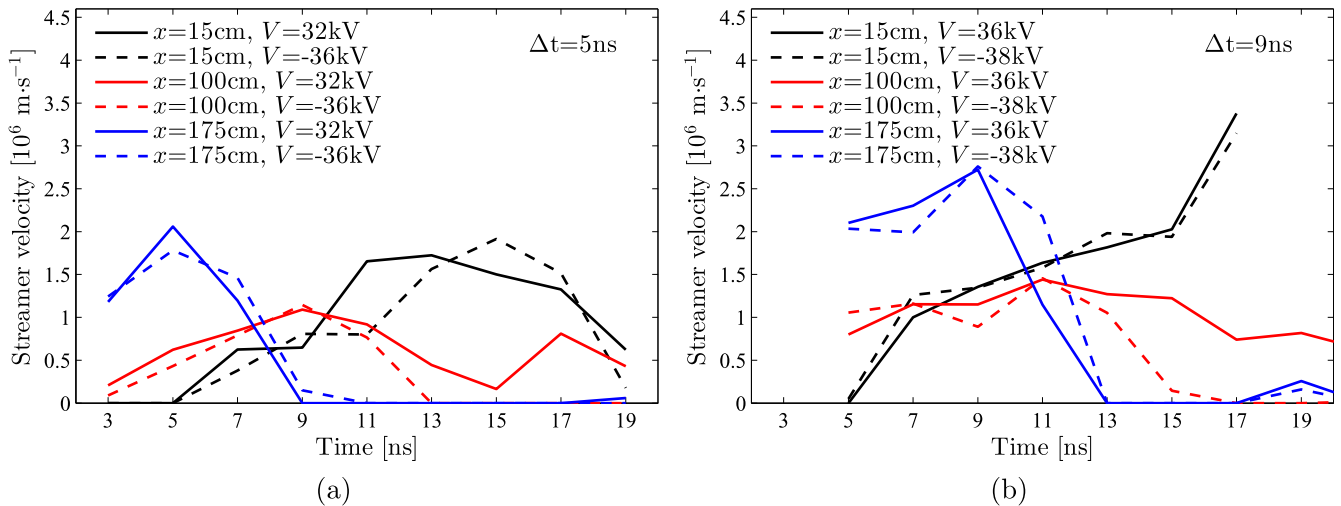


Figure 17. Streamer propagation velocities as a function of time at three different positions in the 2 m reactor for (a) the 5 ns experiments and (b) the 9 ns experiments. The velocities were calculated from the streamer length results of figure 16. For averaging purposes the results for $x = 15$ cm and $x = 175$ cm also include the results of 5 cm on either side of these x -positions. The $x = 100$ cm includes the results of 10 cm on either side ($x = 100$ cm itself is not included because of the reactor coupling).

streamers start propagating as the pulse arrives (at around $t = 1$ ns) and extinguish a short time after the pulse has passed (at around $t = 7$ ns). A little further into the reactor the streamers propagate slightly less far, because the pulse has lost some of its energy and consequently the voltage (and thus the electric field) will be lower at that position (also shown in figure 15(a)). This behaviour dominates the first 1 m of the reactor. However for $x = 0$ –100 cm the behaviour is different, because the pulse reflects on the open end of the reactor (also shown in figure 15(a)). The effect that the voltage is now present for a longer time and that the voltage is higher can clearly be seen in the length of the streamers. Even though the pulse has already dissipated part of its energy in propagating along the reactor, the voltage-doubling at the end of the reactor causes the streamers to propagate further than the streamers in the beginning of the reactor.

The propagation of the 9 ns positive pulse in figure 16(b) is very similar to that of the 5 ns pulse, only now the electric field is present for a longer time due to the longer pulse, which we showed in figure 15(b). This increases the streamer length at all positions, but the analysis that we applied to the 5 ns results applies as well for the 9 ns results. One significant difference is that at the end of measurement (at around 19–21 ns), the streamers are still present over a longer length in the reactor. This is also caused by the longer pulse length.

The general development of the negative discharge (figures 16(c) and (d)) is similar. However, one significant difference is the streamer development at the end of the reactor (low x -position). The positive streamers propagate quite far in the second half of the reactor, which we attributed to the pulse reflection at the end of the reactor. This effect is also present in the negative results, but over a shorter length of the reactor. The reason for this difference is likely the bright discharge at the end of the reactor. This discharge likely dissipates a significant amount of energy, which decreases the pulse voltage and therefore the applied electric field at the end of the reactor.

4.4. Streamer propagation velocity

In the introduction we already mentioned that a higher applied voltage generally results in a higher streamer propagation velocity [2–6, 9, 11, 12, 47]. In the streamer-length discussion, we showed that for the 2 m reactor the voltage is highest at the beginning and at the end of the reactor, so we would expect the highest streamer propagation velocities there.

We calculate the streamer propagation velocity v as a function of time delay t_d and x -position directly from the streamer-length results as

$$v(x, t_d) = \frac{s_{x,t_d} - s_{x,t_d-1}}{t_d - t_{d-1}}, \quad (5)$$

where s_{x,t_d} is the streamer length at time t_d and s_{x,t_d-1} is the streamer length at time t_{d-1} (one delay time previously).

Figure 17 shows the streamer velocity at different positions and pulse polarities in the reactor for the 5 ns measurements (figure 17(a)) and the 9 ns measurements (figure 17(b)). The figures show that our assumptions about the streamer velocities are correct: the velocities are highest at the beginning and at the end of the reactor. In general, the streamer velocities are in the same range of 10^5 – 10^7 m s⁻¹ as other studies.

In the 5 ns results on streamer development, there was no streamer crossing observed in the reactor. Therefore, the streamer velocities show an increase when the streamers initiate, followed by a relatively flat section until the streamers quench. Only at $x = 175$ cm does the velocity start at a high value before dropping. This is because the streamers are already propagating at that position at $t = 3$ ns. As expected, the velocity in the middle of the reactor is lower due to the lower voltage at that position.

There is very little difference between the positive and the negative streamer velocities. The only difference is the velocity at $x = 100$ cm after $t = 9$ ns, which is due to the difference in streamer length at that point.

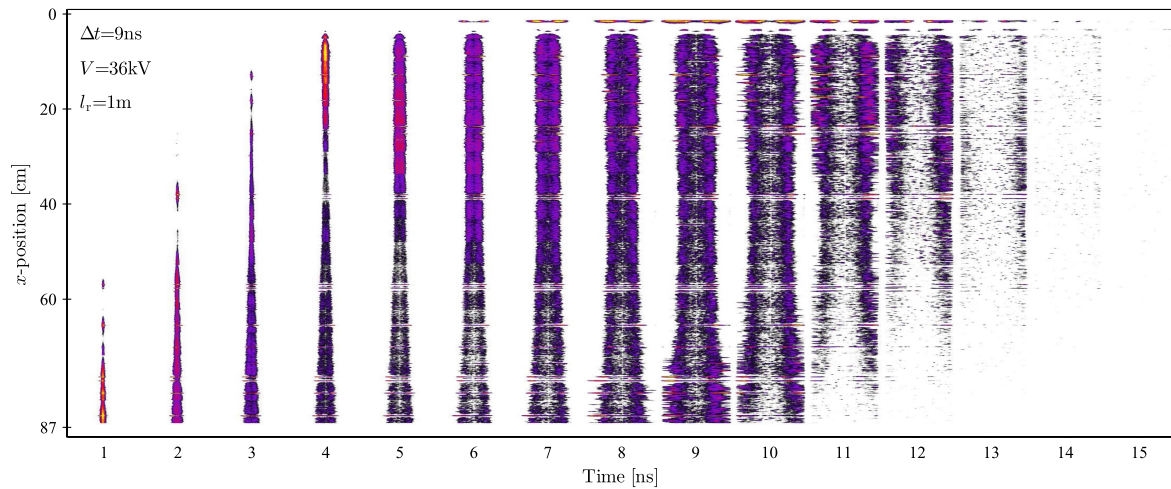


Figure 18. Streamer development in time for a 9 ns positive pulse. The exposure time is 1 ns for all images and each image is the average of 20 photos at each position.

The 9 ns results are similar to the 5 ns results, except now the streamers reach the outer electrode for $x = 15$ cm, which is evident from the sharp increase in velocity at $t = 15$ ns. Also, the velocities are slightly higher for the 9 ns pulse than the 5 ns pulse. This can be explained by the increased time for which the voltage is present for 9 ns pulses; for the 5 ns pulses the voltage drops again when the pulses are not very far across the distance between the electrodes.

The result that there is no significant difference between the velocities of negative and positive streamers is remarkable, considering that most studies show that negative streamers are slower [6, 10, 12, 40, 45–48, 74]. However, some show that the differences between positive and negative streamers become smaller for high applied electric fields and higher rise rates. For instance, Briels *et al* showed in a point-plate geometry that at high pulsed voltages (above 50 kV with a rise time of 15 ns), the velocities of negative streamers were only slightly lower than for positive streamers [10]. Furthermore, Winands *et al* showed that in their wire-plate reactor the velocities of positive and negative streamers were significantly different for pulses with a rise rate of 1.5 kV ns^{-1} , but appeared to become similar for both polarities when the rise rate increases to 2 kV ns^{-1} [6]. Additionally, Wang *et al* showed a similar effect in a corona-plasma reactor when they compared results from two studies [12, 74]. As the results of all these studies use slower pulses, we are unable to directly compare our subnanosecond results.

5. Results: pulse duration variation in a 1 m reactor

In this section we will discuss the results of short-exposure experiments on a 1 m reactor, followed by results of long-exposure experiments. In the short-exposure experiments we used a 1 ns exposure time for all images, steps of 1 ns in the shutter delay time and a camera gain of 980 V.

5.1. ICCD images

We performed short-exposure experiments for 9 ns pulses (positive and negative) and a positive 5 ns pulse. Figure 18 shows the ICCD results for the 9 ns positive pulse (the results for the negative 9 ns pulse were almost the same, if only slightly less bright).

This time there is also a bright reactor-ended discharge for the positive pulses, which were absent in the 2 m positive results (they are also present in the negative results and are larger and brighter there). Furthermore, the streamer distribution is much more homogeneous at all times and positions in the reactor as compared with the 2 m results, which indicates that for a shorter reactor the pulse reflections become less of a defining factor for the 9 ns pulse. However, the results of the positive 5 ns pulse still show longer streamers at the end of the reactor, as we will see in the next sections. In other words: the longer the reactor is, the longer the pulses have to be to achieve a homogeneous streamer distribution at all times and positions in the reactor.

5.2. SPICE simulations

Figure 19 shows SPICE simulation results of the voltage in the 1 m reactor as a function of position and time. Just like the streamer lengths, the maximum voltage in the 1 m reactor for the 9 ns pulse is much more homogeneous than in the 2 m reactor. The voltage in the 1 m reactor for the 5 ns pulse still shows higher values at the end of the reactor. Due to a shorter length over which the pulse can attenuate, the voltage at the end of the reactor is higher for the 1 m results than the 2 m reactor.

5.3. Streamer length and propagation velocity

Figures 20(a) and (b) show the streamer lengths for the 1 m experiments for the positive 5 ns pulse and 9 ns pulse respectively (the differences between the results of the positive and negative 9 ns experiments was almost negligible).

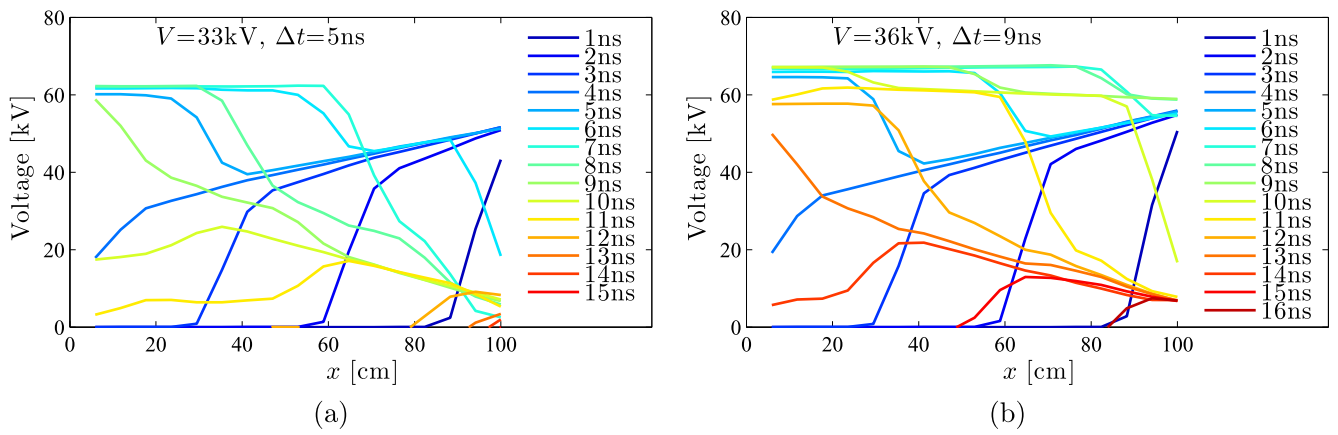


Figure 19. SPICE simulation results for (a) a 5 ns positive pulse and (b) a 9 ns positive pulse at the same applied pulse amplitude as in the 1 m reactor experiments. The figures show the voltage amplitude in the reactor at each position and as a function of time.

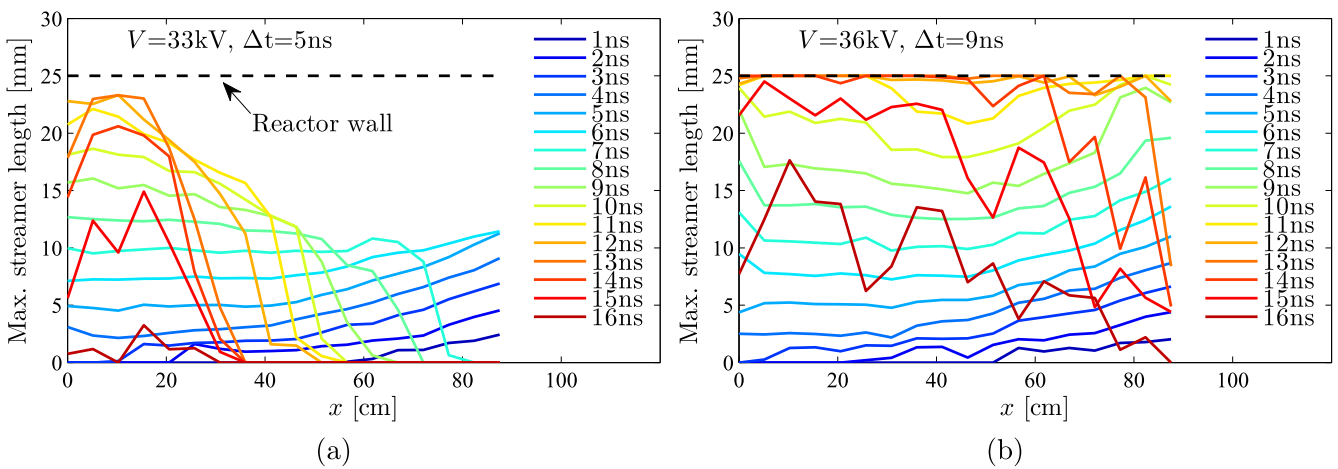


Figure 20. A quantitative representation of the maximum streamer lengths (averaged over the results of 20 photos at each position and each time) calculated from the ICCD images for (a) the positive 5 ns experiments and (b) the positive 9 ns experiments.

The streamer distribution in the reactor is quite homogeneous at all times and positions in the reactor for the streamers generated with the 9 ns pulses. The results show a slight dip in the middle of the reactor, but this dip is not nearly as pronounced as with the 2 m reactor. These results agree well with the SPICE simulations in figure 19(b), which show a more homogenous voltage along the reactor than the 2 m results.

Figure 20(a) now clearly shows that a 5 ns pulse is not long enough to achieve a homogeneous streamer distribution, which was also reflected in the simulated voltages in figure 19(a). However, the streamers in the 5 ns experiments propagate further towards the reactor wall at the end of the 1 m reactor than the 2 m reactor. This is due to the increased voltage at the end of the reactor because now the pulse attenuation is less at the end of the reactor (because it is shorter). Also the 9 ns results show longer streamers on average due to higher voltages than the 9 ns results in the 2 m reactor.

In figure 21, we show the streamer propagation velocity of the streamers in the 9 ns experiments (both polarities). In general, the results are very similar as those of the 2 m reactor, only now the streamers also reach the outer cylinder of the

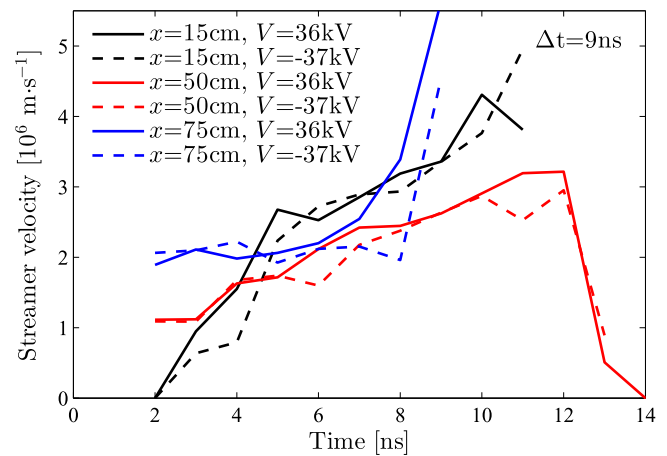


Figure 21. The streamer propagation velocities at different positions in the reactor for the positive 9 ns results of the 1 m reactor.

reactor at the beginning of the reactor (high x -position). Because the bright reactor-ended discharge streamers was now present at both polarities, the streamer velocity results are even more identical than for the 2 m reactor. One

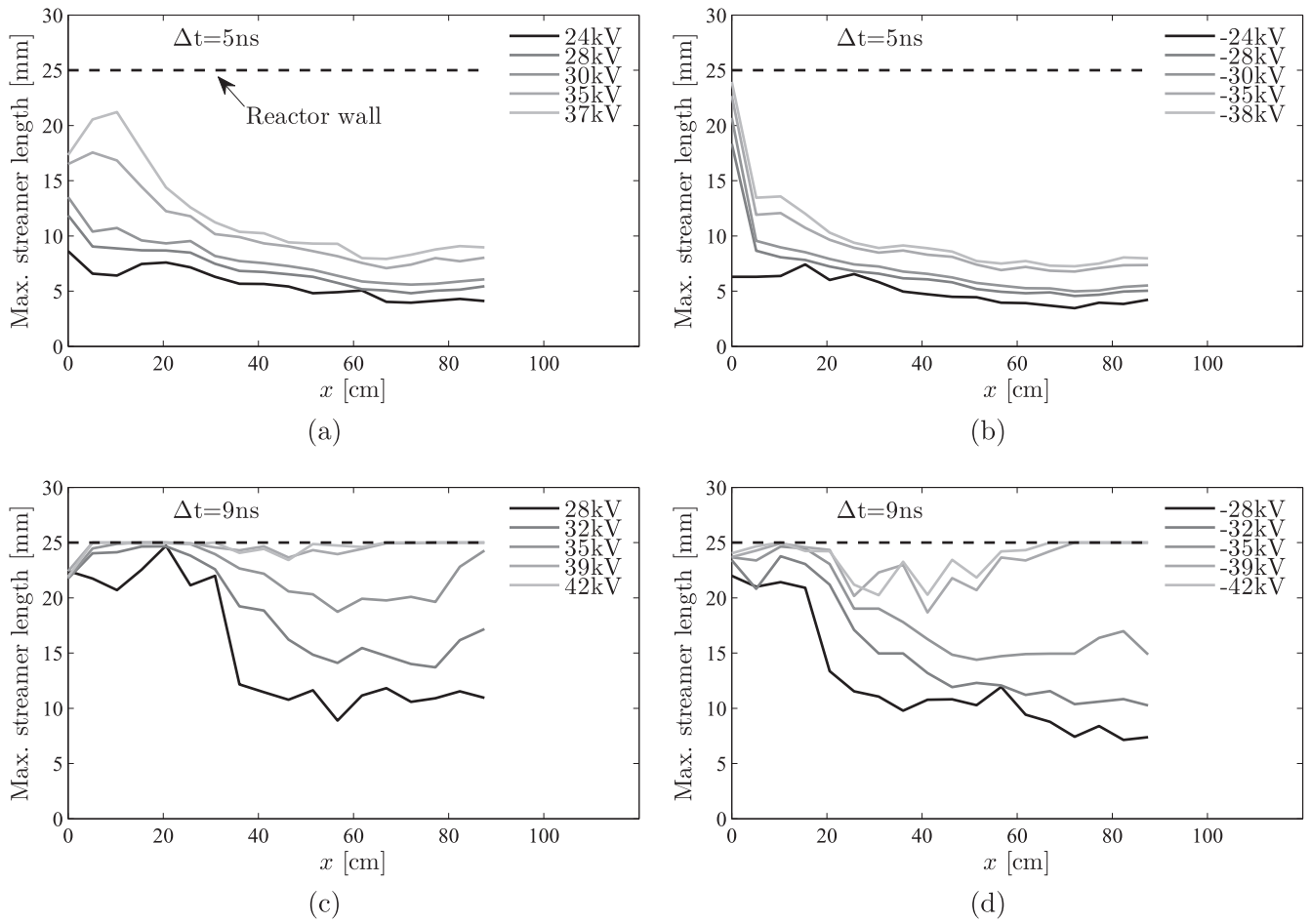


Figure 22. The results of the long-exposure experiments for (a) a positive 5 ns pulse, (b) a negative 5 ns pulse, (c) a positive 9 ns pulse and (d) a negative 9 ns pulse. The results show the streamer length as a function of voltage and position in the reactor.

significant difference between the 1 and 2 m results is that the streamer velocity at the end of the reactor is higher in the 1 m reactor, which is the result of the higher voltage at the end of the reactor as compared to the 2 m reactor.

5.4. Streamer profiles

A disadvantage of the short-exposure experiments is the large amount of time the experiments cost and therefore we only performed these for a limited range of pulse parameters. However, it would be very insightful if we could obtain the streamer distribution for different voltage amplitudes. Therefore, we performed long-exposure experiments. In these experiments we trade time information for voltage flexibility. We took images at an exposure time of 100 ns and a camera gain of 760 V and consequently captured the whole discharge in each image. At each position, we captured 100 images for averaging purposes. From these images, we calculated the maximum streamer lengths at each position, just as with the short-exposure experiments. Figure 22 shows the resulting profiles that indicate what distance the streamers travelled.

The 5 ns results show that the profile shapes scale with the voltage and that the streamer lengths for the positive voltages are slightly larger than the negative voltages. The streamer crossing at $x = 0$ cm for the negative voltages

indicates that there is a reactor-ended bright discharge present at the end of the reactor. This might again increase the energy dissipation at the end of the reactor, which can lead to slightly shorter streamers. Another explanation could be that for lower applied voltages the differences in propagation velocity between positive and negative streamers become similar to what other researchers found, but without the time information we are unable to comment on this with the results of our long-exposure measurements.

The results for the 9 ns pulse duration at the highest voltages are comparable with what we already saw in the results of the short-exposure experiments. However, for lower voltages the homogeneity of the streamer distribution becomes worse for the negative voltages (when compared with the positive voltages). At these lower voltages the pulse propagation through the reactor becomes an important factor again and the results become similar to what we saw in the 2 m reactor for higher voltages.

6. Results: rise-time variation

In this section, we investigate the effect of the rise time of the pulses on the streamer development in the 1 m reactor.

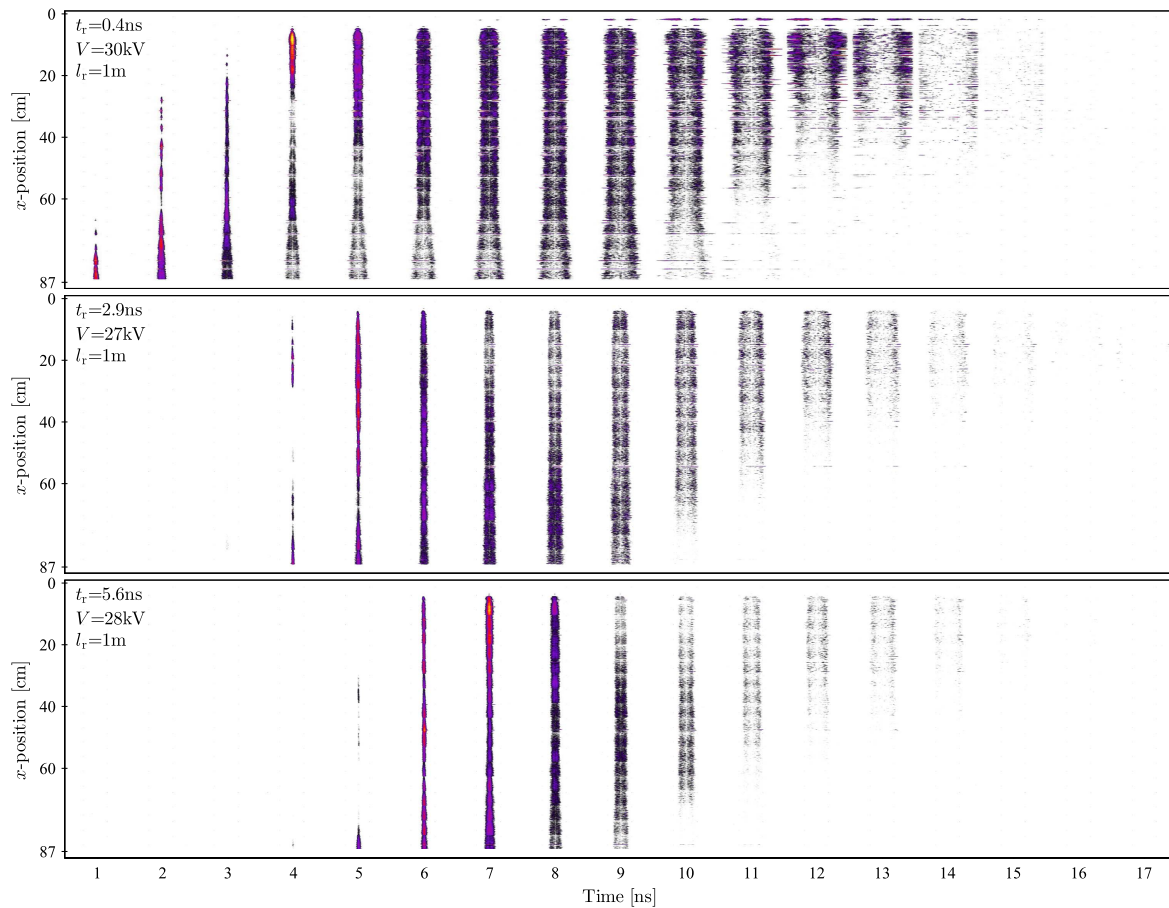


Figure 23. Streamer development in time in the 1 m reactor for a 9 ns positive pulse with three different rise times: 0.4 ns (top), 2.9 ns (middle) and 5.6 ns (bottom). The exposure time is 1 ns for all images and each image is the average of 20 photos at each position.

In the introduction, we mentioned the previous work that was performed on streamer investigation with the rise rate as a parameter. The main conclusion appeared to be that the streamer propagation velocity is higher when a high rise-rate pulse is applied.

We varied the rise time of the pulses with the method that we described in section 2.4. We use three different rise times of the 9 ns pulse in this section: 0.4, 2.9 and 5.6 ns. Two other time scales to keep in mind is the time it takes for the front of the high-voltage pulse to propagate up and down the reactor (6.7 ns) and the time it takes on average for a streamer to cross from the high-voltage wire to the outer wall (8–9 ns for the 9 ns, 0.4 ns rise time pulses). Combined with the used (positive) voltages the used rise times result in rise rates of around 75 kV ns^{-1} , 9 kV ns^{-1} and 5 kV ns^{-1} respectively. For each of these settings we performed short-exposure experiments. The exposure times of the images is 1 ns, the shutter delay was incremented in steps of 1 ns and the gain of the camera was again 980 V.

6.1. ICCD images

Figure 23 shows the ICCD images for the three different rise-time experiments. The figure shows that there is a smaller discharge when the rise rate decreases. Furthermore, where

the streamers initiate immediately for the 0.4 ns rise-time pulse, it takes at least 3 ns longer for the streamers to show for the 5.6 ns rise-time pulse. This delay is due to the longer time it takes for the electric field to increase in the reactor than the shorter rise-time pulses. Therefore, it takes longer for the streamers to initiate at a low rise rate.

Another observation from the ICCD images is that the bright reactor-ended discharge at the end of the reactor only appears for the 0.4 ns rise-time results. This indicates that the voltage at the end of the reactor is higher at that setting than when longer rise-time pulses are used.

6.2. Streamer length and propagation velocity

Figures 24(a) and (b) show the streamer-length results of the ICCD images for the fastest and slowest rise-time pulses. The results show significantly shorter streamers when the rise rate decreases, but also that the streamers are longest at the end of the reactor regardless of the rise rate. This indicates that even for the longer rise times the pulse propagation effects through the reactor remain important.

Figure 25 shows the velocity at $x = 15 \text{ cm}$ for the three different rise-time pulses. The 0.4 ns rise-time result is much like in the previous section, but the velocities for the longer rise times are significantly lower.

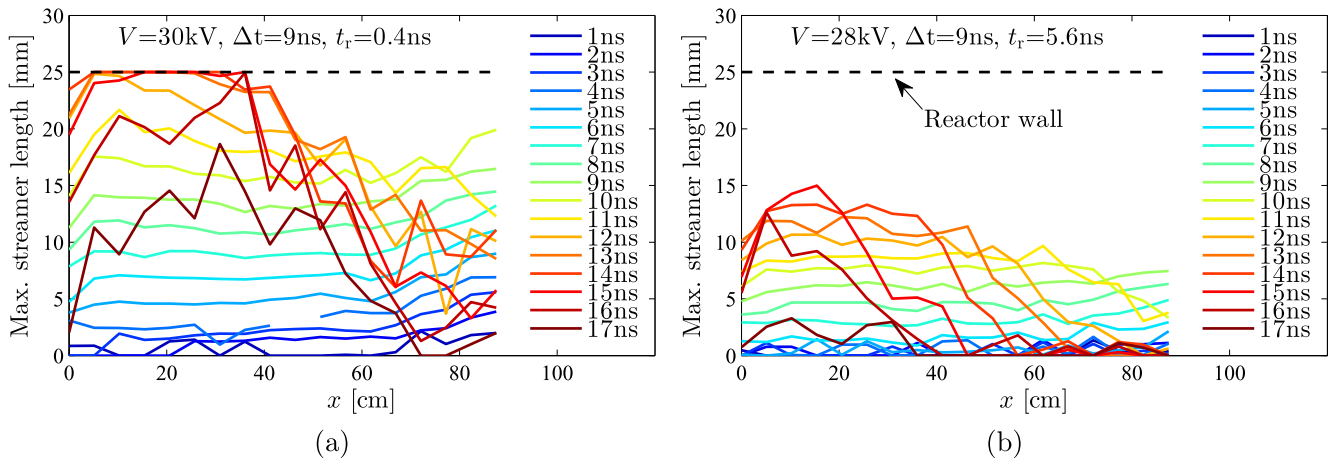


Figure 24. A quantitative representation of the maximum streamer lengths (averaged over the results of 20 photos at each position and each time) calculated from the results of figure 23 for (a) the 0.4 ns rise-time experiments and (b) the 5.6 ns rise-time experiments.

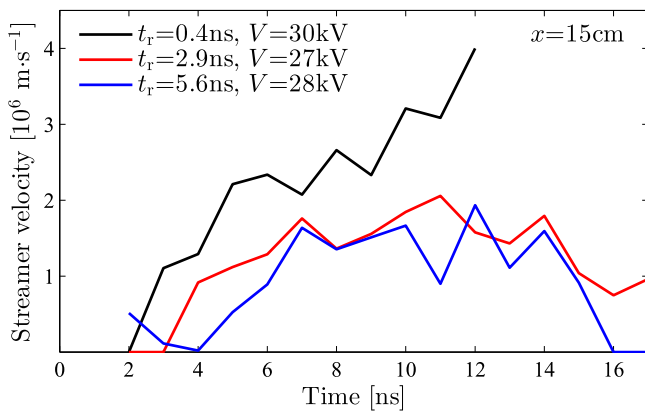


Figure 25. The streamer propagation velocities at $x = 15$ cm for the three different rise times.

Three significant reasons why the velocities are likely higher for the higher rise-rate pulses are listed below.

- The first reason is that it takes some time for a discharge to initiate, and therefore when the voltage rises over a long time, the streamers initiate before the complete voltage is applied across the gap [6, 39, 51]. As a result, it takes a while before the streamer experiences the maximum electric field. With the short rise-time pulses the complete voltage will be across the gap almost immediately and therefore, the streamers experience the maximum electric field almost immediately.
- The second reason originates from the pulse reflection in the reactor. When the 0.4 ns rise-time pulse reflects at the end of the reactor, it adds to itself and almost doubles in voltage. When the 5.6 ns rise-time pulse reflects at this position, it also adds to itself, but due to the relatively long rise-time (it is comparable to the 6.7 ns it takes for the front of the pulse to propagate up and down the reactor) the voltage will not double, but will be significantly lower. This can be seen from the SPICE simulation results of figure 26. From these simulations we can also see that it takes much longer for the complete

voltage to be applied to the reactor at each position for the longer rise-time pulses.

- The last possible reason for the higher streamer propagation velocity is that the electron density in the streamers can become higher for the shorter rise-time pulses. The discharge will be cylinder-symmetrically homogeneous in its very first stages after applying the electric field. An ionisation cloud can form, but the ICCD results showed that there is no significant-sized cloud visible in our experiments. Therefore this homogeneous first stage of the discharge will be extremely short before it destabilises into streamers. However, in this first stage the electron density can grow to a higher value when the external electric field is applied in a shorter time (as compared to a slower rise-time pulse) [51, 75]. The electron density in the generated streamers will consequently also be higher which means that the conductivity of the streamer is higher. A higher-conductivity channel will then result in a higher field enhancement at the streamer head because the voltage drop across the streamer will be lower.

7. Summary and conclusions

In this paper, we investigated the development of streamers in a wire-cylinder reactor to study the effect of reactor length, pulse duration, pulse amplitude, pulse polarity and pulse rise time on the generated streamers. More specifically we were interested in the distribution of the streamers in the reactor to relate this to results of plasma-processing experiments. We studied the streamers by ICCD imaging with a fully automated setup. With this setup, we were able to image the streamers in the entire reactor as a function of time and position in the reactor. From the images, we calculated streamer lengths and streamer propagation velocities. We also developed a SPICE model of the reactor to support the analysis of the streamer development results.

From the results of measurements in a 2 m reactor, we can conclude that the voltage in the reactor at each position

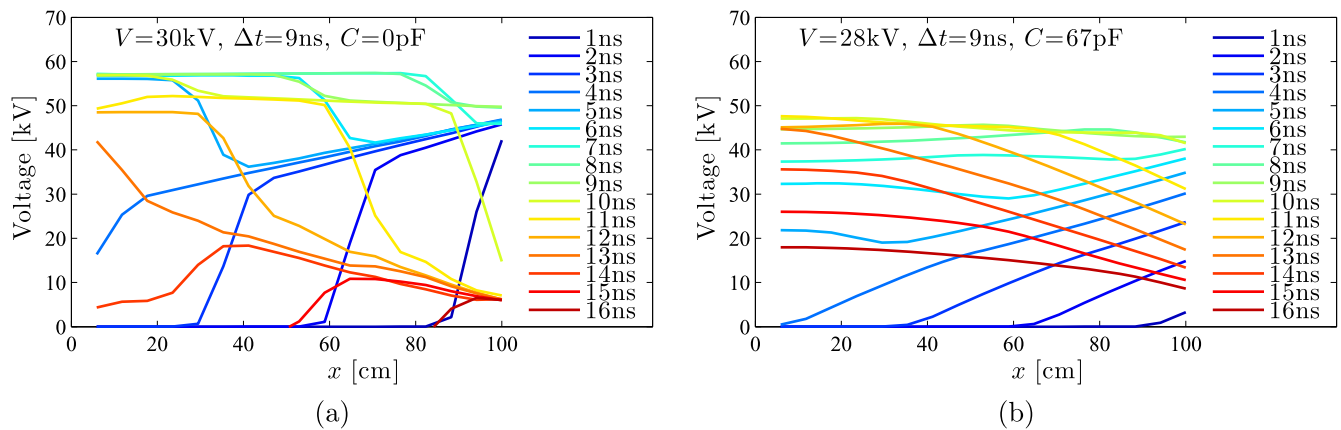


Figure 26. SPICE simulation results for (a) the 0.4 ns rise-time experiments and (b) the 5.6 ns rise-time experiments in the 1 m reactor. The figures show the voltage amplitude in the reactor at each position and as a function of time.

and at each time is the result of a complex interaction with the discharge and the reactor and that the streamer length is related to it (the highest voltage for the longest time results in the longest streamers). Therefore, to obtain the most homogeneous streamer distribution at all times and positions in the reactor, the voltage in the reactor should be as constant as possible at all positions and moments in time, which is not the case in the 2 m reactor and will likely only be worse for even longer reactors (due to the increased dependency of pulse propagation and dissipation). Furthermore, there is very little difference between the negative and positive pulse experiments. As a result, the streamer propagation velocities of the negative and positive streamers are near identical.

In the short-exposure experiments on the 1 m reactor, the streamer distribution is more homogeneous than in the 2 m reactor, which indicates that for a shorter reactor the pulse propagation effects become less significant when similar pulses are used. However, the pulse propagation effects still dominate the streamer development, especially for the shorter 5 ns pulses. Due to the shorter reactor, the voltage at different positions in the reactor remains higher and more constant in time than in the 2 m reactor and consequently, on average, the streamer lengths and velocities are higher. However, from the long-exposure experiments we see that for lower applied voltages the streamer distribution is still not homogeneous for a 1 m reactor.

Finally, streamers generated with a high rise rate propagate farther than streamers generated with a lower rise rate due to a higher streamer velocity and faster start. This higher streamer velocity is the result of a higher voltage at which the streamers initiate at higher rise rates and the overall higher voltage in the reactor due to a larger effect of pulse reflections.

Acknowledgments

This work was supported by the Dutch Technology Foundation STW under contract number 10751.

References

- [1] Fridman A, Chirokov A and Gutsol A 2005 *J. Phys. D: Appl. Phys.* **38** R1
- [2] Blom P P M 1997 High-power pulsed corona *PhD Thesis* Eindhoven University of Technology <http://alexandria.tue.nl/extral/PRF14A/9702338.pdf>
- [3] Briels T M P, Van Veldhuizen E M and Ebert U 2008 *J. Phys. D: Appl. Phys.* **41** 234008
- [4] Tardiveau P, Marode E and Agneray A 2002 *J. Phys. D: Appl. Phys.* **35** 2823
- [5] Ono R and Oda T 2003 *J. Phys. D: Appl. Phys.* **36** 1952
- [6] Winands G J J, Liu Z, Pemen A J M, Van Heesch E J M and Yan K 2008 *J. Phys. D: Appl. Phys.* **41** 234001
- [7] Zhao L, Luo Z Y, Xuan J Y, Jiang J P, Gao X and Cen K F 2012 *IEEE Trans. Plasma Sci.* **40** 802–10
- [8] Krasnochub A V, Nudnova M M and Starikovskii A Y 2005 Cathode-directed streamer development in air at different pressures *43rd AIAA Aerospace Sciences Meeting and Exhibit, Reno, NV, AIAA Paper* vol 1196, p 2005
- [9] Nijdam S, Van De Wetering F M J H, Blanc R, Van Veldhuizen E M and Ebert U 2010 *J. Phys. D: Appl. Phys.* **43** 145204
- [10] Briels T M P, Kos J, Winands G J J, Van Veldhuizen E M and Ebert U 2008 *J. Phys. D: Appl. Phys.* **41** 234004
- [11] Namihira T, Wang D, Katsuki S, Hackam R and Akiyama H 2003 *IEEE Trans. Plasma Sci.* **31** 1091–4
- [12] Wang D, Jikuya M, Yoshida S, Namihira T, Katsuki S and Akiyama H 2007 *IEEE Trans. Plasma Sci.* **35** 1098–103
- [13] Kim H H 2004 *Plasma Process. Polym.* **1** 91–110
- [14] Samukawa S et al 2012 *J. Phys. D: Appl. Phys.* **45** 253001
- [15] Huiskamp T 2015 Nanosecond pulsed power technology for transient plasma generation *PhD Thesis* Eindhoven University of Technology <https://pure.tue.nl/ws/files/3809268/798746.pdf>
- [16] van Heesch E J M, Winands G J J and Pemen A J M 2008 *J. Phys. D: Appl. Phys.* **41** 234015
- [17] Matsumoto T, Wang D, Namihira T and Akiyama H 2010 *IEEE Trans. Plasma Sci.* **38** 2639–43
- [18] Wang D, Namihira T and Akiyama H 2011 *J. Adv. Oxid. Technol.* **14** 131–7
- [19] Matsumoto T, Wang D, Namihira T and Akiyama H 2011 *Japan. J. Appl. Phys.* **50** 08JF14
- [20] Fujiwara M 2006 *Japan. J. Appl. Phys.* **45** 948
- [21] Kakuta T, Yagi I and Takaki K 2015 *Japan. J. Appl. Phys.* **54** 01AG02
- [22] Ono R, Nakagawa Y and Oda T 2011 *J. Phys. D: Appl. Phys.* **44** 485201

- [23] Namihira T, Tsukamoto S, Wang D, Katsuki S, Hackam R, Akiyama H, Uchida Y and Koike M 2000 *IEEE Trans. Plasma Sci.* **28** 434–42
- [24] Huiskamp T, Voeten S J, van Heesch E J M and Pemen A J M 2014 *IEEE Trans. Plasma Sci.* **42** 127–37
- [25] Huiskamp T, Beckers F J C M, van Heesch E J M and Pemen A J M 2014 *IEEE Trans. Plasma Sci.* **42** 859–67
- [26] Huiskamp T, van Heesch E J M and Pemen A J M 2015 *IEEE Trans. Plasma Sci.* **43** 444–51
- [27] Huiskamp T, Beckers F J C M, van Heesch E J M and Pemen A J M 2013 *IEEE Trans. Plasma Sci.* **41** 3666–74
- [28] Komuro A, Ono R and Oda T 2012 *J. Phys. D: Appl. Phys.* **45** 265201
- [29] Eichwald O, Ducasse O, Dubois D, Abahazem A, Merbahi N, Benhenni M and Yousfi M 2008 *J. Phys. D: Appl. Phys.* **41** 234002
- [30] Creighton Y L M, Van Veldhuizen E M and Rutgers W R 1994 *IEE Proc., Sci. Meas. Technol.* **141** 141–7
- [31] Dubrovin D, Nijdam S, Clevis T T J, Heijmans L C J, Ebert U, Yair Y and Price C 2015 *J. Phys. D: Appl. Phys.* **48** 055205
- [32] Ono R, Tobaru C, Teramoto Y and Oda T 2009 *Plasma Sources Sci. Technol.* **18** 025006
- [33] Pancheshnyi S V, Sobakin S V, Starikovskaya S M and Starikovskii A Y 2000 *Plasma Phys. Rep.* **26** 1054–65
- [34] Naidis G V 2010 *Plasma Sources Sci. Technol.* **19** 055010
- [35] Marode E 1975 *J. Appl. Phys.* **46** 2005–15
- [36] Ono R and Oda T 2004 *J. Phys. D: Appl. Phys.* **37** 730
- [37] Komuro A, Takahashi K and Ando A 2015 *J. Phys. D: Appl. Phys.* **48** 215203
- [38] Nijdam S, Wormeester G, van Veldhuizen E M and Ebert U 2011 *J. Phys. D: Appl. Phys.* **44** 455201
- [39] Briels T M P, Kos J, van Veldhuizen E M and Ebert U 2006 *J. Phys. D: Appl. Phys.* **39** 5201
- [40] Teramoto Y, Fukumoto Y, Ono R and Oda T 2011 *IEEE Trans. Plasma Sci.* **39** 2218–9
- [41] Yagi I, Okada S, Matsumoto T, Wang D, Namihira T and Takaki K 2011 *IEEE Trans. Plasma Sci.* **39** 2232–3
- [42] Komuro A, Ono R and Oda T 2013 *Plasma Sources Sci. Technol.* **22** 045002
- [43] Pancheshnyi S, Nudnova M and Starikovskii A 2005 *Phys. Rev. E* **71** 016407
- [44] Chen S, Heijmans L C J, Zeng R, Nijdam S and Ebert U 2015 *J. Phys. D: Appl. Phys.* **48** 175201
- [45] Yoshinaga K, Okada S, Wang D, Namihira T, Katsuki S and Akiyama H 2009 *Acta Phys. Pol. A* **115** 1050
- [46] Luque A, Ratushnaya V and Ebert U 2008 *J. Phys. D: Appl. Phys.* **41** 234005
- [47] Won J Y and Williams P F 2002 *J. Phys. D: Appl. Phys.* **35** 205
- [48] Vasilyak L M, Vetchinin S P and Polyakov D N 1999 *Tech. Phys. Lett.* **25** 749–51
- [49] Wormeester G, Pancheshnyi S, Luque A, Nijdam S and Ebert U 2010 *J. Phys. D: Appl. Phys.* **43** 505201
- [50] Ebert U, van Saarloos W and Caroli C 1997 *Phys. Rev. E* **55** 1530
- [51] Babaeva N Y and Naidis G V 2016 *IEEE Trans. Plasma Sci.* **44** 899–902
- [52] Beckers F J C M, Pemen A J M and Heesch V E J M 2014 *IEEE Trans. Plasma Sci.* **42** 2404–5
- [53] Beckers F J C M, Hoeben W F L M, Huiskamp T, Pemen A J M and van Heesch E J M 2013 *IEEE Trans. Plasma Sci.* **41** 2920–5
- [54] Beckers F J C M, Hoeben W F L M, Pemen A J M and Van Heesch E J M 2013 *J. Phys. D: Appl. Phys.* **46** 295201
- [55] Ma H and Qiu Y 2003 *Ozone Sci. Eng.* **25** 127–35
- [56] Namihira T, Tsukamoto S, Wang D, Hori H, Katsuki S, Hackam R, Akiyama H, Shimizu M and Yokoyama K 2001 *IEEE Trans. Plasma Sci.* **29** 592–8
- [57] McAdams R 2007 *Plasma Sources Sci. Technol.* **16** 703
- [58] Van Veldhuizen E M, Rutgers W R and Bityurin V A 1996 *Plasma Chem. Plasma Process.* **16** 227–47
- [59] Puchkarev V and Gundersen M 1997 *Appl. Phys. Lett.* **71** 3364–6
- [60] Pokryvailo A, Yankelevich Y, Nissim N, Baksht R and Ashkenazy J 2006 *IEEE Trans. Plasma Sci.* **34** 104–14
- [61] van Heesch E J M, Dageinckx M H P, van Gompel F M and Blom P P M 1995 Surge corona propagating along a transmission line *Proc. 9th Int. Symp. on High Voltage Engineering (Graz, Austria, 28 August–1 September 1995)*
- [62] Beckers F J C M 2015 Pulsed power driven industrial plasma processing *PhD Thesis* Eindhoven University of Technology <http://repository.tue.nl/801599>
- [63] Huiskamp T, Sengers W and Pemen A J M 2016 *Rev. Sci. Instrum.* **87** 123509
- [64] Huiskamp T, Beckers F J C M, van Heesch E J M and Pemen A J M 2016 *IEEE Sens. J.* **16** 3792–801
- [65] Huiskamp T, Beckers F J C M, Hoeben W F L M, van Heesch E J M and Pemen A J M 2016 *Plasma Sources Sci. Technol.* **25** 054006
- [66] LTspice IV <http://linear.com/designtools/software/#LTspice> (Accessed: 01 May 2017)
- [67] Naudé N, Cambronne J P, Gherardi N and Massines F 2005 *Eur. Phys. J. Appl. Phys.* **29** 173–80
- [68] El-Deib A A, Dawson F, Bhosle S and Zissis G 2010 *IEEE Trans. Plasma Sci.* **38** 2260–73
- [69] Wigington R L and Nahman N S 1957 *Proc. IRE* **45** 166–74
- [70] Van Veldhuizen E M and Rutgers W R 2003 *J. Phys. D: Appl. Phys.* **36** 2692
- [71] Huiskamp T, Brok W J M, Stevens A A E, van Heesch E J M and Pemen A J M 2012 *IEEE Trans. Plasma Sci.* **40** 1913–25
- [72] Pokryvailo A et al 2006 *IEEE Trans. Plasma Sci.* **34** 1731–43
- [73] Kuffel J, Kuffel E and Zaengl W S 2000 *High Voltage Engineering Fundamentals* (Oxford: Newnes)
- [74] Wang D, Namihira T and Akiyama H 2011 *IEEE Trans. Plasma Sci.* **39** 2268–9
- [75] Teunissen J, Sun A and Ebert U 2014 *J. Phys. D: Appl. Phys.* **47** 365203